Mesoderm-specific transcript reduces ciliary sphingomyelin levels to promote tendon stem/progenitor cells osteochondrogenesis in traumatic heterotopic ossification

Authors: Bowen Lai[1†], Yuan Gao[1†], Zhilong Shen[2], Jianquan Zhao[1], Heng Jiang[1*], Xuhui Zhou[1,3*]

Affiliations:

[1]Department of Orthopedics, The Second Affiliated Hospital of Naval Medical University; Shanghai, 200003, China.

[2]Department of Orthopedic Oncology, The Second Affiliated Hospital of Naval Medical University; Shanghai, 200003, China.

[3]Translational Research Centre of Orthopedics, Shanghai General Hospital, Shanghai Jiao Tong University School of Medicine; Shanghai, 200080, China.

*Corresponding author. Email: include the email addresses of the corresponding author(s). Please use the asterisk (*) symbol for the corresponding author information.

† These authors contributed equally to this work.

One Sentence Summary: novel mechanisms and potential therapeutic strategies of traumatic heterotopic ossification

Abstract: Traumatic heterotopic ossification (tHO) is a prevalent musculoskeletal disorder with ectopic bone forms in soft tissues post-trauma. Despite its substantial impact on patients, which may range from local discomfort to severe functional impairments, the etiology and underlying mechanisms of tHO remain unknown, and no treatments have been demonstrated to be effective for tHO. Here, we found that ciliary Hedgehog (Hh) and PI3K-Akt signaling in tendon-derived stem/progenitor cells (TSPCs) is upregulated during tHO development, leading to the activation of GLI family zinc finger 2 (GLI2) transcription factor, which promotes mesoderm-specific transcript (MEST) gene expression. We further showed that MEST can change ciliary lipids composition and reduce the abundance of sphingomyelin in cilia, creating a positive feedback loop that amplifies ciliary Hh signaling, enhancing the osteogenesis and chondrogenesis of TSPCs and driving tHO. Cilia suppression by knocking down ciliary genes intraflagellar transport 88 (IFT88) or ADP ribosylation factor like GTPase 3 (ARL3), or using the SMO inhibitor vismodegib, restores normal TSPCs osteo-chondrogenic differentiation via downregulating Hh signaling. Inhibiting MEST expression or adding exogenous sphingomyelin in vivo also effectively alleviate tHO. These findings deepen our understanding of tHO pathogenesis and provide novel insights to develop novel therapeutic strategies against tHO.

Main Text:

INTRODUCTION

Traumatic heterotopic ossification (tHO) is a common musculoskeletal disorder characterized by the formation of ectopic bone in soft tissues, affecting a significant proportion of patients who experience severe injuries or orthopedic procedures(*1*). Although most cases of tHO present with localized symptoms such as pain, swelling, and restricted joint movement,

severe cases can lead to significant functional impairments, including joint ankylosis and chronic disability, necessitating intensive surgical interventions like amputation(*2*). However, the etiology and underlying biological mechanisms of tHO remain unknown. Notably, there are no effective drugs available that can specifically eliminate ectopic bone formation or decelerate the progression of tHO. Therefore, it is necessary to conduct more studies exploring the molecular mechanisms of tHO to provide new strategies for clinical treatment that alleviate the suffering of patients and the burden on medical resources.

Primary cilia are solitary, non-motile microtubule-based organelles that protrude from the cell surface, acting as essential sensory antennae for cells to receive and transduce extracellular signals(*3*). They play crucial roles in various developmental and physiological processes, including embryonic patterning, tissue homeostasis, and cellular differentiation(*4*). Recent studies have increasingly highlighted the involvement of primary cilia in skeletal biology. For instance, primary cilia in osteocyte function as critical mechanosensors to maintain normal bone formation and help to treat osteoporosis(*5*). Our previous study found that primary cilia can positively regulate the process of osteochondral differentiation of stem cells from patients with fibrodysplasia ossificans progressiva (FOP), a genetic form of HO caused by gene point mutations(*6*). However, there is currently no research involving the function and regulatory mechanisms of primary cilia in the pathogenesis of tHO.

The recruitment of stem/progenitor cells and their differentiation into osteoblasts or chondrocytes are key steps in the formation of tHO(*7*). Tendon stem/progenitor cells (TSPCs) are located between the long and parallel collagen fiber chains of tendon and are surrounded by the extracellular matrix(*8*). TSPCs can differentiate into tenocyte tissue (tendon) and non-tenocyte tissues (such as bone, cartilage, and adipose tissue) in different circumstances. Studies have reported that the increased ectopic bone volume in Achilles tendon of rats is accompanied with increased bone morphogenetic protein (BMP) expression and enhanced osteogenesis in TSPCs(*9*). Moreover, the inhibition of the mTOR signaling by rapamycin treatment can suppress the osteochondral differentiation of TSPCs and tHO(*10*). Thus, it is important to explore whether primary cilia regulate the abnormal osteochondrogenic differentiation in TSPCs and how primary cilia contribute to the progression of tHO via specific mechanisms.

MEST (mesoderm-specific transcript) is an imprinted gene predominantly expressed from the paternal allele. The protein encoded by it is widely expressed in mesodermal tissues, belongs to the α/β hydrolase superfamily, and has enzymatic activity. Through high-throughput sequencing technology, we indicated that MEST might be a key downstream molecule in the regulation of tHO by primary cilia. Studies have confirmed that knocking down MEST in human periodontal ligament stem cells will inhibit the expression of their stem cell markers and proliferation ability and weaken their multi-lineage differentiation abilities. However, no study focuses on whether MEST is involved in regulating TSPCs osteogenic or chondrogenic differentiation. Therefore, it is necessary to explore the role of MEST in the development of tHO and the possibility of targeting MEST as a novel therapeutic strategy.

There is a diffusion barrier in the transition zone at the base of the primary cilia, which can restrict the free movement of proteins and lipids in and out of the cilia, resulting in differences in the composition of proteins and lipids on the ciliary membrane and the cytoplasmic membrane. Under the stimulation of mechanical stress or chemical signals, the selective movement of specific lipids in and out of the cilia can dynamically influence the function of receptors on the ciliary surface and the activity of downstream signaling pathways, thereby regulating cell proliferation and differentiation(*11*). The disruption of the homeostasis of ciliary lipids has been

reported to be associated with a variety of diseases. Some studies have reported that abnormalities in genes encoding key enzymes involved in cholesterol metabolism can lead to defects in the formation of primary cilia in osteoblasts and in the differentiation of osteoblasts, resulting in craniofacial malformation(*12, 13*). Since MEST has been found to possess the characteristics of lipase, which can promote the hypertrophy of adipocytes and expand the volume of adipose tissue(*14*), the regulation of lipid changes within the cilia of TSPCs by MEST may be an important part of the pathogenesis of tHO.

In this study, we demonstrated that the activity of ciliary Hh and PI3K-Akt signaling of TSPCs is significantly upregulated during tHO development, leading to the activation and nuclear translocation of the transcription factor GLI2, which promotes the expression of the MEST gene. The upregulation of MEST expression results in a reduction of sphingomyelin abundance within the primary cilia, which in turn amplifies the activation of the ciliary Hh signaling. This forms a positive feedback loop that significantly enhances the osteogenic and chondrogenic differentiation potential of TSPCs, thereby driving local ectopic bone deposition and contributing to the development and progression of tHO. Moreover, knockdown ciliary gene or suppressing Hh signaling restored the TSPCs differentiation. Inhibiting MEST expression or adding exogenous sphingomyelin in vivo also had great therapeutic effects on tHO. Unraveling these mechanisms may enhance our understanding of the pathogenesis of tHO and pave the way for the development of innovative and effective therapeutic approaches.

RESULTS

1. Inhibition of ciliary function alleviates the formation of tHO

To induce tHO, 6- to 8-week-old male C57BL/6 mice were subjected to a burn injury using a 60°C heated aluminum block on the dorsal skin, followed by resection of the right Achilles tendon (Figure 1a). Tendon tissues from the injured sites were harvested at 0 days (prior to injury), and at 3, 7, 21, and 56 days after injury for subsequent histological examination (Figure 1b). HE staining demonstrated disorganized and irregular tendon fibrous tissue at 3 to 7 days post-injury. Chondrogenic structures were detected at 21 days, and osteogenic structures were observed at 56 days. Masson trichrome staining showed blue-stained tendon collagen fibers, with the progression of structural disorganization and tHO being similar to that observed with HE staining. Von Kossa staining revealed the appearance of brown calcified nodules at 21 days, which became deeply stained by 56 days, suggesting calcium deposition due to new bone formation.

To explore the function of cilia in tHO, we performed immunofluorescence staining on tendon tissues collected from mice at 0, 3, 7, 21, and 56 days post-injury (Figure 1c). ARL13B, a specific marker for primary cilia, was used to quantify ciliated cells. The percentage of ARL13B-positive cells was 27.21% in the control group (0 days post-injury). After injury, the proportion of ARL13B-positive cells increased to 40.14% at 3 days, 38.07% at 7 days, and 39.75% at 21 days, before declining to 33.62% at 56 days. These data indicated that ciliated cells increased rapidly during tHO and may contribute to its development (Figure 1d). To further identify the potential specific cell types targeted by cilia in the process of tHO, immunofluorescence double-staining was performed on tendon tissue samples collected at various time points post-injury. The following marker pairs were used: ARL13B with CD31 (endothelial cells marker), ARL13B with F4/80 (macrophages marker), ARL13B with PDGFRα (stem/progenitor cells marker), ARL13B with TNMD (tendon cells marker), and ARL13B with α-SMA (smooth muscle cells marker). Immunofluorescence analysis revealed clear co-localization between ARL13B and

PDGFRα after tHO injury (Figure 1c). Quantitatively, the proportion of ARL13B+PDGFRα+cells was the highest among the five double-staining groups. Specifically, the percentage of ARL13B+PDGFRα+cells was 55.91% in the control group. After injury, this proportion significantly increased to 95.29% at 3 days, 85.56% at 7 days, 90.17% at 21 days, and 95.49% at 56 days (Figure 1e, f). These data indicate that cilia mainly affect tHO by targeting stem/progenitor cells.

Intraflagellar transport protein 88 homolog (IFT88) functions as a core protein of the IFT-B complex, driving anterograde transport within cilia. Arf-like Protein 3 (ARL3), a small GTPase, is involved in ciliogenesis and the maintenance of ciliary function. To locally inhibit ciliary function, we administered adeno-associated virus (AAV) vectors carrying *shIft88* and *shArl3* via intramuscular injection into the lower limbs of mice with tHO. The results showed that knockdown of *Ift88* and *Arl3* significantly decreased the bone volume of ectopic bone formation, whereas bone density was not significantly altered. This suggests that inhibition of ciliary function can reduce the severity of tHO (Figure 1g).

2. Primary cilia in stem/progenitor cells contribute to tHO progression

Single-cell RNA sequencing (scRNA-seq) can distinguish differences among individual cells in a high-throughput manner, thereby clarifying cellular heterogeneity and underlying molecular mechanisms during disease progression. Therefore, in our study, we reanalyzed a scRNA-seq dataset (GSE126060) from mouse tHO tissues. The dataset included 12 samples, with three samples per group at four time points: pre-injury (Day 0) and post-injury (Day 3, Day 7, and Day 21). The UMAP plot showed a total of 21,880 cells detected and divided into nine subclusters (Figure 2a) according to the previous study(*15*). Bubble plot revealed the marker genes of each cluster, and markers for the Mesenchymal cluster were Pdgfra and Prrx1 (Figure 2b, c). Group-stratified UMAP plots revealed that, as tHO progresses, the percentage of Macrophage cluster cells peaked at 3 days (74.43%) post-injury, later rapidly reduced to 37.10% at 7 days and 15.02% at 21 days post-injury, indicating the evolution of the local inflammatory phase (Figure 2d). In contrast, the Mesenchymal cluster cells exhibited a larger proportion at 7 (43.44%) and 21 days (49.43%), suggesting that the osteogenic and chondrogenic differentiation of stem/progenitor cells contributes to tHO during this period (Figure 2d). Consequently, we analyzed the differentially expressed genes in the Mesenchymal subcluster at 7 and 21 days post-injury compared with the control group and revealed that 82 genes were upregulated in the Mesenchymal subcluster at Day 7, and 53 genes were upregulated at Day 21 (Figure 2e). Since the knockdown of ciliary genes *Ift88* and *Arl3* can alleviate tHO formation in vivo, we are interested in the expression of ciliary genes at single-cell level. *Ift88* has low expression at single cell level likely due to limited scRNA-seq depth, but still predominantly localizes to the mesymenchal subpopulation, and shows a subtle upward trend during tHO (Figure S1). We then shifted our focus to another ciliary gene IFT20 which is also a component of the IFT-B complex and has been reported to regulate ciliogenesis and skeletal development(*16*). It can be shown that both *Ift20* and *Arl3* are highly expressed in the Mesenchymal cluster (Figure 2f). Moreover, with the developmnet of tHO after injury, the expression of *Ift20* and *Arl3* in Mesencymal cluster rapidly increased in Day 7 and Day 21 group, while the trends over time were not significant in other clusters (Figure 2g). The results indicated primary cilia and ciliary genes may mainly functioned in stem/progenitor cell (like TSPCs as we identified above) during the progression of tHO.

3. Primary cilia regulate the osteochondrogenic differentiation potential of TSPCs

Since the above results suggested that cilia on stem/progenitor cells may regulate tHO, and considering that abnormal differentiation of tendon stem/progenitor cells (TSPCs) has been reported to potentially contribute to the pathogenesis of tHO(*17, 18*), we isolated TSPCs from the tendon tissues of C57BL/6 mice. Microscopic examination showed that these TSPCs exhibited a fibroblast-like spindle-shaped morphology (Figure 3a). Flow cytometry analysis demonstrated that 88.1% of the TSPCs were double-positive for Pdgfrα and Prrx1 (consistent with the scRNA-seq results), thereby confirming the stem/progenitor cell characteristics of the isolated TSPCs (Figure 3b).

To investigate the regulatory effects of cilia on the functions of TSPCs, we transfected lentivirus vectors carrying *shIft88* and *shArl3* into mouse TSPCs to establish stable transfectants with knockdown of ciliary genes. qPCR and Western blot analyses confirmed successful knockdown of *Ift88* and *Arl3*, indicating that these transfectants were suitable for subsequent experiments (Figure S2). Immunofluorescence staining for ARL13B and α-tubulin (Acetyl Lys40) was used to observe changes of primary cilia in TSPCs following knockdown of cilia. The results showed a significant reduction in cilia counts and length (Figure 3c). Quantitative analysis revealed that the proportion of ciliated TSPCs was approximately 53.54% in the control group but decreased to 19.36% in the *shIft88* group and 34.70% in the *shArl3* group, indicating a marked decrease in cilia number in TSPCs following ciliary gene knockdown. Additionally, the average cilia length was 3.37 μm in the control group but reduced to 2.06 μm in the *shIft88* group and 2.14 μm in the *shArl3* group, demonstrating a significant shortening of cilia length in TSPCs after ciliary gene knockdown (Figure 3d, e).

Previous studies have shown that the osteogenic and chondrogenic differentiation capabilities of TSPCs are abnormally activated during the process of tHO, leading to the formation of ectopic bone in tendon tissues(*18*). Therefore, investigating whether cilia can regulate the osteogenic and chondrogenic differentiation of TSPCs is important for exploring the regulatory mechanisms of cilia in tHO. We induced osteogenic differentiation in mouse TSPCs and performed alizarin red staining after 21 days of induction. Compared with the control group, the alizarin red staining was lighter in the *shIft88* and *shArl3* groups, indicating less calcium deposition (Figure 3f, S2). This suggests that knockdown of ciliary genes attenuates the osteogenic differentiation capacity of TSPCs. qPCR analysis revealed that the expression of osteogenic differentiation-related genes *Alpl*, *Bglap*, and *Sp7* was significantly reduced in the *shIft88* and *shArl3* groups compared with the control group, while *Runx2* expression remained largely unchanged (Figure 3g). These findings further confirm a positive correlation between cilia function and the osteogenic differentiation capacity of TSPCs. Similarly, we induced chondrogenic differentiation in the stable transfectants of mouse TSPCs with ciliary gene knockdown and performed alcian blue staining after 21 days. Compared with the control group, the blue staining was lighter (Figure 3f, S3). Meanwhile, qPCR analysis revealed that the expression of chondrogenic differentiation-related genes *Col2a1* and *Acan* was significantly reduced, while *Sox9* expression retained (Figure 3g). These results indicate that primary cilia may positively modulate the osteogenic and chondrogenic differentiation of TSPCs, leading to abnormal osteogenesis and chondrogenesis in local soft tissues and ultimately resulting in tHO.

4. Primary cilia modulate MEST expression to promote tHO

To further identify key genes involved in tHO and their potential crosstalk with primary cilia, we obtained bulk-RNA sequencing data from a public database for mouse tHO tissues (GSE233201) (Figure 4a). We then integrated these data with RNA sequencing results from TSPCs with ciliary gene *Ift88* knockdown and control groups to identify common differentially expressed genes (Figure 4b). Genes upregulated in the Mesenchymal cluster at 7 and 21 days during tHO (GSE126060), genes upregulated in injured tissue at 21 days of tHO (GSE233201), and genes downregulated in TSPCs with ciliary gene *Ift88* knockdown were obtained respectively (Table S1). Venn diagram analysis identified three common differentially expressed genes: MEST, PTN, and COL2A1 among these three datasets (Figure 4c). COL2A1 is a key gene for chondrogenic differentiation, while PTN showed insignificant differences after validation (Figure S4). Thus, we focused on the role of the MEST gene in tHO in subsequent studies. scRNA-seq analysis revealed that *Mest* is predominantly expressed in the Mesenchymal cluster (Figure 4d). Both qPCR and Western blot analyses demonstrated a significant reduction in *Mest* RNA and protein expression following knockdown of the ciliary genes *Ift88* or *Arl3* (Figure 4e, f). Moreover, scRNA-seq analysis showed that the expression of *Mest* in the Mesenchymal cluster exhibits an upward trend with the progression of tHO (Figure 4g). Consistently, Immunohistochemical analysis of tendon tissues at various time points after establishment of tHO further showed that MEST protein expression is progressively upregulated during the tHO development (Figure 4h), suggesting that MEST may play a significant role in the regulatory mechanisms of tHO. Notably, immunofluorescence staining showed no significant co-localization between MEST and α-tubulin (Figure 4i), indicating that MEST likely functions outside the cilia in TSPCs to influence their function and thereby contribute to the occurrence and progression of tHO.

5. MEST facilitates the TSPCs differentiation and tHO in a ciliary localization-independent manner

As MEST is primarily not localized or expressed on the cilia of TSPCs, we explored how MEST can regulate tHO in a cilia localization-independent manner. We constructed two small interfering RNAs (siRNAs): *siMest-1* and *siMest-2*, to inhibit *Mest* gene expression in vitro. qPCR analysis revealed a significant decrease in *Mest* expression following *siMest* intervention, confirming that *siMest* can effectively suppress MEST function (Figure 5b). Alizarin red staining showed that the *siMest* group exhibited lighter staining and fewer calcium nodules compared with the control group after 21 days of osteogenic differentiation induction (Figure 5a, S5). Additionally, the expression of osteogenic differentiation-related genes *Alpl, Runx2* and *Bglap* was significantly reduced (Figure 5b). Similarly, alcian blue staining after 21 days of chondrogenic differentiation induction showed that, compared with the control group, the *siMest* group exhibited lighter staining and reduced chondrogenic capacity (Figure 5a, S5). The expression of chondrogenic differentiation-related genes *Sox9, Col2a1*, and *Acan* was also decreased (Figure 5b). Moreover, we divided the Mesenchymal cluster to Mest-high and Mest-low subclusters based on the expression level of Mest in tHO scRNA-seq data (Figure 5c). Though *Alpl, Sp7,* and *Col2a1* were not significantly expressed between two subclusters probably because of their extreme low expression in single-cell level (Figure S6), the expression of *Runx2, Sox9,* and *Acan* were greatly higher in Mest-high subcluster, which further demonstrated our results. These findings indicate that MEST promotes the TSPCs

osteochondrogenesis and inhibiting MEST function can diminish the osteogenic and chondrogenic differentiation capacity of TSPCs in tHO.

We further employed immunofluorescence staining with α-tubulin to label the cilia of TSPCs in the control and *siMest* groups (Figure 5c). Quantitative analyses showed no significant difference in cilia number (58.26% vs 53.11%), while cilia length was significantly shorter in the *siMest* group compared with the control group (2.46 μm vs 3.48 μm) (Figure 5d). In addition, we performed in vivo experiments by locally injecting a AAV vector carrying *shMest* into mice with tHO to knock down *Mest* expression in local tissues. Micro-CT imaging revealed that the volume of ectopic new bone in the *shMest* group was significantly lower than that in the control group, while bone density remained largely unchanged (Figure 5e, f). Collectively, these results suggest that MEST are involved in regulating the ciliary function of TSPCs and their osteochondrogenic differentiation in a ciliary localization-dependent manner. Inhibition of *Mest* expression in the specific way may serve as a potential therapeutic target for treating tHO.

6. MEST targets ciliary Hh and PI3K-Akt signaling to mediate TSPCs differentiation in tHO

To further investigate the specific molecular mechanisms and downstream targets through which cilia regulate tHO, we conducted enrichment analysis on our previously obtained sequencing data. Gene Ontology (GO) enrichment analysis showed that differentially expressed genes at the site of tHO 21 days post-injury were significantly enriched in functions related to the extracellular matrix and ossification (Figure 6a). Consistent with these findings, differentially expressed genes in TSPCs following knockdown of cilia-related genes were also enriched in ossification (Figure 6b). These results suggest a strong correlation between the differentially expressed genes and tHO, indicating that gene engineering therapies targeting these genes may represent a potential strategy for treating tHO. We further conducted Gene Set Enrichment Analysis (GSEA) on the differentially expressed genes in TSPCs following knockdown of cilia-related genes, and the results showed significant enrichment in the Hh signaling pathway (Figure 6c). Given that the activity of the Hedgehog (Hh) signaling pathway is dependent on the primary cilia for regulating embryonic development and tissue differentiation, and considering that aberrant upregulation of Hh has been implicated in the pathogenesis of tHO following injury(*19*), the Hh signaling activity within TSPCs cilia is likely closely related to tHO. Additionally, KEGG enrichment analysis indicated that differentially expressed genes in the Mesenchymal cluster of tHO tissues, as well as those in TSPCs following knockdown of ciliary gene *Ift88*, were significantly enriched in the PI3K-Akt signaling pathway (Figure 6d, e). To verify the bioinformatics analysis results, we performed qPCR and found that the mRNA expression of key Hh signaling molecules *Shh* and *Ptch1* was significantly downregulated in TSPCs undergoing osteogenic and chondrogenic differentiation after *shIft88* or *shArl3* treatment (Figure 6f). Western blot analysis also demonstrated a significant reduction in the protein expression of SHH and PTCH1 (Figure 6g). Additionally, during the osteogenic and chondrogenic differentiation of TSPCs, the ratios of phosphorylated PI3K to total PI3K (p-PI3K/PI3K) and phosphorylated AKT to total AKT (p-AKT/AKT) were significantly decreased following ciliary gene knockdown (Figure 6g), indicating reduced phosphorylation of PI3K and AKT and thus inhibition of the PI3K-Akt signaling pathway. Smoothened (SMO) is a key seven-transmembrane receptor involved in Hh signaling and is inhibited by PTCH1 when Hh signaling is inactive. Upon binding of the Hh ligand to PTCH1, the inhibitory effect of PTCH on SMO is alleviated, thereby

enabling the activation of SMO. Interestingly, scRNA-seq analysis showed that *Smo* mainly expressed and increased over time in Mesenchymal cluster (Figure 6h, i) after trauma, further demonstrating the Hh signaling was activated in tHO development. Collectively, these results suggest that the primary cilia of TSPCs may lead to aberrant activation of the Hh and PI3K-Akt signaling pathways, thereby promoting osteogenic and chondrogenic differentiation of TSPCs and exacerbating tHO.

Previous results have confirmed that MEST can influence the osteogenic and chondrogenic differentiation of TSPCs and regulate tHO in ciliary localization-independent manner, yet the underlying molecular mechanisms remain unclear. qPCR (Figure S7) and Western blot (Figure 7a) analyses indicated that, compared with the control group, the expression levels of key Hh signaling molecules SHH and PTCH1 were significantly downregulated at both the mRNA and protein levels in *siMest*-transfected TSPCs undergoing osteogenic and chondrogenic differentiation. In addition, the phosphorylation levels of PI3K and AKT were also decreased (Figure 7b). These findings suggest that MEST may promote the osteogenic and chondrogenic differentiation of TSPCs and the formation of tHO by mediating the Hh and PI3K-Akt signaling pathways. GLI2, a key transcriptional activator of the Hh signaling pathway, translocate to the nucleus upon Hh signal activation and induces the expression of downstream genes involved in cell proliferation and differentiation. The sequence logo of GLI2 transcription factor was shown and the JASPAR database predicts that the GLI2 can bind to the MEST gene promoter at positions 904-916 and 1698-1710, thereby activating MEST transcription and enhancing its expression (Figure 7c). Dual-luciferase reporter assays using pGL4.10 as vector demonstrated that GLI2 can bind to the MEST promoter at both predicted sites, with overexpression of GLI2 significantly increasing luciferase activity, thus confirming that GLI2 positively regulates Mest transcription (Figure 7d). To further elucidate the regulatory role of the GLI2 transcription factor in tHO, we performed immunohistochemistry on tendon tissues obtained from mice with tHO and found that GLI2 expression progressively increased with the development of the ossification (Figure 7e). Meanwhile, qPCR and Western blot analyses revealed that, compared with the control group, the *Gli2* mRNA and protein expression levels of GLI2 were significantly downregulated in TSPCs undergoing osteogenic and chondrogenic differentiation after knockdown of ciliary genes (Figure 7f, g). Moreover, in vivo experiments involving local injection of a AAV vector carrying *shMest* into mice with tHO to knockdown *Mest* expression showed decreased protein expression levels of GLI2, PTCH1, and SMO, as shown by immunohistochemistry (Figure 7h), indicating that targeting Mest may alleviate the occurrence and progression of tHO by reducing the activation level of the Hh signaling pathway. Collectively, these results suggest a self-amplifying loop of GLI2 and MEST via Hedgehog signaling that promotes the osteogenic and chondrogenic differentiation of TSPCs, and thereby exacerbates the tHO phenotype.

7. MEST reduced ciliary sphingomyelin levels in TSPCs

Recent studies have shown that ciliary lipids play a crucial role in maintaining ciliary structure stability and regulating ciliary mechanosensation and signal transduction. Aberrant distribution and dynamic changes in ciliary lipids have been implicated in various diseases, including polycystic kidney disease(*20*) and obesity(*21*). Moreover, deficiencies in key cholesterol-metabolizing enzymes have been shown to cause ciliary defects that impact bone development(*13*). These findings have prompted our interest in investigating the changes in lipids within TSPCs cilia during tHO. We first isolated cilia from TSPCs in the control and

357 *siMest* groups using ultracentrifugation to prepare ciliary suspensions (for more details see
358 Methods). Immunofluorescence confirmed that the cilia were effectively removed from TSPCs
359 after treatment (Figure 8a). Then we conducted Untargeted lipidomics using liquid
360 chromatography-tandem mass spectrometry (LC-MS/MS) on the collected ciliary suspensions.
361 OPLS-DA analysis showed obvious differences in the lipid profiles of TSPCs cilia between the
362 control (NC) and *siMest* (SIM) groups (Figure 8b). We performed differential analysis of lipids
363 based on the LIPID MAPS® classification system and the differential expressed primary (Figure
364 8c, d) and secondary (Figure S8a) lipids were classified. Totally, we screened 159 upregulated
365 and 157 downregulated lipids in the SIM group with the criteria of |log2FC| > 1 and P value <
366 0.05 (Table S2, Figure 8e, S8b). Compared with the NC group, the abundance of sphingomyelin
367 (SM) within the cilia of TSPCs in the SIM group was significantly increased, while the content
368 of triglycerides (TG) was significantly decreased (Figure 8f). Heatmaps revealed consistent
369 differential changes in almost all subclasses of sphingomyelins and triglycerides, including 22
370 sphingomyelins and 53 triglycerides (Figure S8c). To further explore how the differentially
371 expressed lipids within the cilia of TSPCs might contribute to tHO, we conducted KEGG
372 pathway enrichment analysis. Consistent with our prior findings, the differentially expressed
373 metabolites were enriched in pathways including glycerophospholipid metabolism, sphingolipid
374 signaling, and sphingolipid metabolism (Figure 8g, S8d).
375 SGMS2 (sphingomyelin synthase 2) gene encodes sphingomyelin synthase 2, which is
376 mainly involved in the synthesis of sphingomyelin on the cell membrane. It has been reported
377 that SGMS2-mediated sphingomyelin metabolism was involved in skeletal homeostasis
378 regulation and its mutation could lead to a series of bone diseases like osteoporosis and skeletal
379 dysplasia(*22*). We found that *Sgms2* was mainly expressed in Mesenchymal cluster but rarely
380 expressed in Mest-high subcluster (Figure 8h). Moreover, the expression level of *Sgms2* in Mest-
381 high subcluster gradually reduced over time after tHO at single-cell level (Figure 8i), indicating
382 that Mest reduced ciliary sphingomyelin synthesis in tHO possibly by inhibiting *Sgms2*
383 expression in TSPCs. These results indicated that MEST may reduce the synthesis and
384 abundance of sphingomyelin within the cilia of TSPCs, and that silencing *Mest* expression in
385 vitro can reverse the decrease in sphingomyelins within the cilia of TSPCs.
386
387 **8. Targeting ciliary sphingomyelin in TSPCs rescue tHO development via Hh signaling**

388 Since previous findings have demonstrated that MEST can induce the osteogenic and
389 chondrogenic differentiation of TSPCs in ciliary localization-independent manner, thereby
390 promoting the occurrence and development of tHO, it is essential to explore whether lipids
391 within the cilia of TSPCs also contribute to this pathogenesis. Research has shown that
392 sphingomyelins and cholesterol interact on the cellular membrane to regulate intracellular
393 signaling processes, and their dynamic balance is crucial for maintaining normal cellular
394 functions(*23*). Considering the parallel roles of cholesterol and triglycerides under physiological
395 and pathological conditions, we hypothesize that the decrease in triglycerides within the cilia of
396 TSPCs following *Mest* knockdown may follow the increase in sphingomyelins. Therefore,
397 studying how sphingomyelins regulate TSPCs function is of great significance. We induced
398 osteogenic and chondrogenic differentiation in TSPCs and performed alizarin red and alcian blue
399 staining with different treatments respectively (Figure 9a, b). Compared with the control group,
400 treatment with exogenous sphingomyelin significantly diminished the osteogenic and
401 chondrogenic differentiation capacities, indicating that sphingomyelins can suppress the
402 osteogenic and chondrogenic differentiation of TSPCs. Treatment of TSPCs with myriocin (a

403 sphingomyelin synthesis inhibitor) significantly enhanced the osteogenic and chondrogenic
404 differentiation capacities of TSPCs. However, when sphingomyelins and myriocin were applied
405 together, the osteogenic and chondrogenic differentiation capacities of TSPCs were not
406 significantly different from the control group. Furthermore, downregulation of *Mest* gene
407 expression in TSPCs using *siMest* mitigated the excessive upregulation of osteogenic and
408 chondrogenic differentiation induced by myriocin-mediated reduction in sphingomyelins. qPCR
409 analysis of the expression of osteogenic (*Alpl, Runx2,* and *Bglap*) and chondrogenic (*Col2a1,*
410 *Sox9,* and *Acan*) differentiation-related genes in TSPCs revealed trends consistent with the
411 staining results (Figure 9c), suggesting that inhibiting *Mest* gene expression may increase the
412 sphingomyelin content in TSPCs cilia, thereby attenuating their osteogenic and chondrogenic
413 differentiation capacities and alleviating tHO.
414 Notably, a study has demonstrated that depletion of sphingomyelins on the ciliary membrane
415 can increase the accessibility of cholesterol, thereby amplifying the transmission of the Hh
416 signaling pathway within the cilia(*24*). Therefore, we hypothesize that the results may be
417 associated with the activity of the Hh signaling pathway. Smoothened (SMO), a seven-
418 transmembrane receptor protein, serves as a bridge between Hh ligands and GLI transcription
419 factors in the Hh pathway. Direct targeting of SMO has become a trending area in drug research
420 targeting the Hh signaling pathway, with the SMO inhibitor vismodegib being FDA-approved
421 for the treatment of basal cell carcinoma. When vismodegib was administered to TSPCs treated
422 with myriocin, the osteogenic and chondrogenic differentiation capacities were significantly
423 reduced (Figure 9a, b), and the expression of osteogenic and chondrogenic differentiation-related
424 genes was downregulated, with no significant differences compared to the control group (Figure
425 9c). qPCR analysis of key Hh signaling molecules (*Shh, Ptch1, and Gli2*) during osteogenic
426 differentiation of TSPCs showed that myriocin strongly activated the Hh signaling pathway,
427 while exogenous sphingomyelin had the opposite effect, inhibiting Hh signaling (Figure 9d). In
428 contrast, groups treated with myriocin+sphingomyelin, myriocin+siMest, and
429 myriocin+vismodegib exhibited Hh signaling pathway component gene expression levels that
430 were not significantly different from the control group (Figure 9d). In vivo experiments by local
431 injection of exogenous sphingomyelin into tHO mice injury site revealed that the volume of
432 ectopic bone in mice treated with exogenous sphingomyelin was significantly lower than that in
433 the PBS-injected control group, with no significant differences in bone mineral density between
434 the two groups (Figure 9e). These findings suggest that the depletion of cilia sphingomyelins
435 may facilitate the osteogenic and chondrogenic differentiation of TSPCs through the activation
436 of the Hh signaling pathway, thereby exacerbating tHO. This effect can be attenuated by
437 silencing the MEST gene or using a SMO inhibitor vismodegib, which may represent emerging
438 candidate therapeutic targets for tHO.

439 **DISCUSSION**

440 The formation of traumatic heterotopic ossification (tHO) is a complex process involving the
441 aberrant differentiation of different cells into osteogenic and chondrogenic lineages. Primary
442 cilia are microtubule-based, non-motile organelles that act as cellular antennae, sensing and
443 transducing extracellular signals to regulate various developmental and physiological processes.
444 Several studies have revealed the relationship between primary cilia and skeletal diseases,
445 including defects of skeletal development such as polydactyly(*25*) and craniofacial
446 abnormalities(*12*). Our previous research found that primary cilia in skeletogenic cells is crucial
447 for BMP and ActA-mediated osteogenesis and chondrogenesis and thereby governs the
448 development of fibrodysplasia ossificans progressiva (FOP). In this study, we demonstrate that

449 cilia function is significantly upregulated during tHO, with an increased prevalence of ciliated
450 cells in the injury site, particularly among tendon stem/progenitor cells (TSPCs). This
451 observation aligns with previous studies indicating that primary cilia are essential for tissue
452 repair(*26*) and regeneration(*27*) but extends our understanding by linking cilia activity directly to
453 the pathogenesis of tHO.
454 Our study reveals that primary cilia positively modulate the osteogenic and chondrogenic
455 differentiation of TSPCs, contributing to the development of tHO. Knockdown of cilia-related
456 genes (*Ift88* and *Arl3*) significantly reduced the differentiation capacity of TSPCs, as evidenced
457 by decreased calcium deposition and downregulation of key osteogenic and chondrogenic
458 markers, resulting in reduced ectopic bone volume in tHO mice. This finding is consistent with
459 the established role of primary cilia in regulating stem/progenitor cell functions in various cell
460 types. For examples, loss of Numb (a ciliary protein) in spinal neural progenitors lead to reduced
461 cerebellar size via ciliary Hh signaling in mice(*28*). The Hh signaling pathway, which is cilia-
462 dependent, is known to be aberrantly activated in postnatal skeletogenesis(*29*) and heterotopic
463 ossification in osteoblast(*30*). Meanwhile, inactivated PI3K-Akt signaling after ciliary gene
464 IFT80 deficiency results in decreased odontogenic differentiation in dental pulp stem cells(*31*).
465 Our study further supports this by showing that cilia gene knockdown in TSPCs downregulates
466 Hh signaling components and reduces PI3K-Akt signaling activation, leading to reduced
467 osteogenesis and chondrogenesis. This suggests that primary cilia serve as a crucial regulatory
468 hub, integrating signals that drive the aberrant osteogenic and chondrogenic differentiation of
469 TSPCs during tHO.
470 A significant contribution of our study is the identification of MEST as a core regulator of
471 tHO for the first time. MEST encodes protein that is widely expressed in mesoderm. As we know,
472 the mesoderm develops into the skin, muscle, bone, and other connective tissues in our body,
473 which indicate the potential role of MEST in skeletogenesis. Our scRNA-seq results showed that
474 MEST is predominantly expressed in stem/progenitor cells and is upregulated during tHO
475 progression. A recent study reported that MEST specifically expressed in mesenchymal cells and
476 induced bone formation during mouse digit tip regeneration(*32*). In our study, scRNA-seq
477 showed that the expression levels of osteogenic and chondrogenic genes in Mest highly
478 expressed stem/progenitor cells were higher than Mest low expressed stem/progenitor cells.
479 Moreover, knockdown of MEST in TSPCs attenuated their osteogenic and chondrogenic
480 differentiation capacities, while *shMest* significantly alleviate severity of tHO in mice, indicating
481 a pivotal role of MEST in promoting tHO by regulating TSPCs differentiation. Interestingly,
482 MEST functions in a cilia localization-independent manner, suggesting that it may act
483 downstream of cilia signaling pathways. This finding is innovative as it uncovers a novel
484 regulatory axis involving MEST and highlights its potential as a therapeutic target for tHO.
485 Our study elucidates the molecular mechanisms through which MEST regulates tHO. We
486 demonstrate that MEST modulates the Hh and PI3K-Akt signaling pathways, which are critical
487 for TSPC differentiation. Furthermore, we show that the GLI2 transcription factor, a key
488 activator of the Hh pathway, binds to and promotes MEST transcription. This finding is
489 supported by previous studies indicating that GLI2 is a master regulator of bone homeostasis(*33*)
490 and that its activity is tightly regulated by cilia function(*34*). In summary, the results indicated a
491 positive feedback loop where Hh signaling activates MEST, which in turn enhances TSPC
492 osteogenic and chondrogenic differentiation and tHO progression via Hh and PI3K-Akt signaling.
493 In the presence of external stimuli, the selective influx and efflux of specific lipids in
494 primary cilia can dynamically modulate the functions of cilia and cells(*11*). This process is

intricately linked to adipogenesis(*21*) and diseases such as polycystic kidney disease(*20*). Thus, another novel aspect of our study is the investigation of ciliary lipid metabolism in TSPCs during tHO. By untargeted lipidomic after isolation of primary cilia, we show that MEST regulates the abundance of various important lipids within TSPC cilia, especially with sphingomyelin levels being significantly upregulated upon MEST knockdown. This finding is intriguing as sphingomyelins are known to interact with cholesterol to regulate ciliary signaling processes(*24*). Our study suggests that the balance of sphingomyelins and triglycerides within cilia is crucial for TSPCs differentiation. Specifically, we demonstrated that exogenous sphingomyelin treatment inhibits TSPCs osteogenic and chondrogenic differentiation and reduce ecotopic bone volume in tHO mice. This effect is mediated through the ciliary Hh signaling, as evidenced by the activation of Hh signaling upon myriocin treatment and its inhibition by exogenous sphingomyelin. Vismodegib, a SMO inhibitor targeting Hh signaling, can also diminish osteogenesis and chondrogenesis of TSPCs. These findings provide a new perspective on the role of lipid metabolism in tHO and suggest that targeting ciliary sphingomyelin levels may represent a potential therapeutic strategy.

Several limitations should be acknowledged in the study. First, our study primarily focuses on the role of primary cilia in TSPCs, while other cell types involved in tHO, such as macrophages and endothelial cells, were not extensively investigated. Future studies should explore the cilia-dependent functions of these cells and their interactions with TSPCs during tHO. Second, our in vivo experiments were limited to local injection of AAV vectors carrying *shRNA*, which may not fully recapitulate the complex physiological environment of tHO. Further studies using genetically modified animal models are needed to validate our findings. Third, while we identified MEST as a key regulator of tHO, the detailed molecular mechanisms through which MEST modulates sphingomyelin metabolism within cilia remain unclear. Future studies should investigate the specific interactions between MEST and lipid metabolic enzymes and their impact on cilia function as the regulator of tHO.

The schematic diagram of the study is shown in Figure 10. Our study opens several avenues for future research. First, further investigation into the role of primary cilia in other cell types involved in tHO is warranted. This will provide a more comprehensive understanding of the cellular and molecular mechanisms underlying tHO progression. Second, exploring the therapeutic potential of targeting cilia function or MEST expression in preclinical models of tHO is an important next step. This could involve the development of small molecules or gene therapies aimed at modulating cilia activity or inhibiting MEST function. Third, elucidating the detailed molecular mechanisms through which MEST regulates lipid metabolism within cilia will provide new insights into the pathogenesis of tHO and identify potential therapeutic targets. Finally, translating these findings into clinical applications will require rigorous preclinical and clinical trials to assess the safety and efficacy of cilia-targeted therapies for tHO.

MATERIALS AND METHODS

1. Experimental tHO mice

Male C57/BL6 mice weighing approximately 20 g and aged 6–8 weeks bought from Hangzhou Ziyuan Laboratory Animal Technology Co., Ltd were used for construction of burn/tenotomy tHO mice model as previously reported(*35*). Briefly, mice were anesthetized via intraperitoneal injection of sodium pentobarbital. Hair was removed from the left hind limb (from the knee to the ankle) and a 2×3 cm area on the left side of the midline of the spine using an electric clipper for surgical preparation. A longitudinal incision was made along the Achilles

540 tendon to expose the gastrocnemius tendon, which was then transected transversely. The skin
541 was sutured using 5-0 surgical thread. Subsequently, a 2×3×3 cm aluminum block preheated to
542 60°C in a water bath was applied to the 2×3 cm area on the left side of the midline of the spine
543 for approximately 17 seconds without additional pressure. The surgical site was disinfected with
544 an alcohol swab postoperatively, and mice were housed individually. Antibiotics and analgesics
545 were administered as needed. The success of the tHO model was evaluated 8–10 weeks post-
546 surgery.
547
548 **2. Micro-CT**

549 After euthanasia, the lower leg and foot of the mice were harvested and fixed overnight at
550 4°C in 10% formalin solution. Subsequently, the samples were subjected to high-resolution
551 micro-CT using a SkyScan CT reconstruction software (Bruker Corporation). Three-dimensional
552 modeling and additional data analysis were performed using 3D.SUITE (Bruker Corporation).
553 The entire ectopic bone region of the specimen was selected as the region of interest (ROI) for
554 quantification of bone volume (BV). Additionally, the distal tibial epiphysis of the mouse was
555 selected as the ROI for quantification of bone mineral density (BMD) and trabecular thickness
556 (Tb.Th).
557
558 **3. Immunofluorescence**

559 For immunofluorescence staining of tissues and cells, samples were prepared by fixing in
560 4% paraformaldehyde at 4°C for 24 hours (tissues) or at room temperature for 15 minutes (cells).
561 Tissues were subsequently deparaffinized and rehydrated through gradient ethanol, while cells
562 were permeabilized with ice-cold methanol or 0.3% Triton X-100 (Solarbio Life Sciences) as
563 needed. Both tissues and cells were blocked with 10% normal goat serum or 1% BSA to reduce
564 nonspecific binding. Primary antibodies, raised in different host species, were applied and
565 incubated overnight at 4°C. After washing, fluorophore-conjugated secondary antibodies (#A-
566 11034, Thermo Fisher Scientific) were added and incubated for 1 hour at room temperature in
567 the dark. Nuclei were stained with DAPI for 10–15 minutes, followed by washing. Sections and
568 cells were mounted with an anti-fade medium and imaged using Nikon ECLIPSE Ni microscopic
569 system. Primary antibodies used are as follows: ARL13B (1:500, #17711-1-AP, Proteintech
570 Group Inc.); Acetyl-α-Tubulin (Lys40) (1:800, #12152, Cell Signaling Technology) ; PDGFRα
571 (1:100, #sc-338, Santa Cruz); CD31 (1:500, #11265-1-AP, Proteintech Group Inc.); F4/80 (1:500,
572 #28463-1-AP, Proteintech Group Inc.); TNMD(1:100, #PA5-112767, Invitrogen); α-SMA(1:500,
573 #14395-1-AP, Proteintech Group Inc.); MEST (1:250, #11118-1-AP, Proteintech Group Inc.).
574
575 **4. Histology and immunohistochemistry**

576 Following euthanasia, the tHO mice tendon tissues were collected and fixed in 4%
577 paraformaldehyde at 4°C for 24 hours. After three washes with PBS, the samples were
578 decalcified in 10% EDTA at 4°C for 21 days. The tissues were then embedded in paraffin, and
579 sagittal sections of the Achilles tendon were obtained via paraffin microtomy. Histological
580 staining was performed using hematoxylin and eosin (H&E), Masson's trichrome, and Von
581 Kossa staining to evaluate ectopic ossification in the Achilles tendon. The sections were
582 dehydrated in ethanol, mounted, and imaged using Nikon ECLIPSE Ni microscopic system.
583 For immunohistochemistry on paraffin-embedded sections, the slides were first
584 deparaffinized in xylene and rehydrated through a graded ethanol series. Endogenous peroxidase

585 activity was quenched with 3% hydrogen peroxide in methanol. Antigen retrieval was performed
586 by heating the sections in citrate buffer (pH 6.0) for 10 minutes at 95–100°C. Sections were then
587 blocked with 10% fetal bovine serum or 1% BSA for 1 hour at room temperature. Primary
588 antibodies were applied and incubated either for 1 hour at room temperature or overnight at 4°C,
589 followed by washing with PBS. Secondary antibodies (#Ab205718, abcam) were added and
590 incubated for 30 minutes at room temperature. For visualization, sections were developed with
591 DAB substrate and counterstained with hematoxylin. Finally, the sections were dehydrated,
592 cleared, and mounted with neutral gum for microscopic examination using Nikon ECLIPSE Ni
593 microscopic system. Primary antibodies used are as follows: MEST (1:200, #11118-1-AP,
594 Proteintech Group Inc.), GLI2 (1:200, #28245-1-AP, Proteintech Group Inc.), PTCH1 (1:100,
595 #ab53715, abcam), SMO (1:1000, #20787-1-AP, Proteintech Group Inc.).
596

597 **5. Isolation of TSPCs and cell culture**

598 The isolation of TSPCs was conducted as previously reported(*36*). Briefly, 6- to 8-week-old
599 C57/BL6 mice were sacrificed, and their entire gastrocnemius tendons were aseptically harvested.
600 The tendons were washed three times with 1X PBS and finely minced using ophthalmic scissors.
601 The minced tissue was collected in a 15 ml centrifuge tube and digested with 3 ml of 3 mg/ml
602 collagenase type I (#SCR103, Sigma-Aldrich) at 37°C in a shaking incubator for 45 minutes.
603 The mixture was then centrifuged at 500 rpm for 5 minutes to remove the collagenase.
604 Subsequently, the pellet was resuspended in 3 ml of 2 U/ml dispase type II (#4942078001,
605 Roche) and digested at 37°C for another 45 minutes. After centrifugation at 500 rpm for 1
606 minute to remove the dispase, the cell pellet was resuspended in 3 ml of low-glucose DMEM
607 supplemented with 10% fetal bovine serum (FBS) and 1% penicillin/streptomycin. The cell
608 suspension was filtered through a 70 μm cell strainer into a 10 cm culture dish and supplemented
609 with 6-8 ml of complete culture medium. The medium was changed for the first time after 3 days
610 and then every other day. When the cells reached 80% confluence (7-10 days later), they were
611 passaged for further experimental use.
612

613 **6. Virus and siRNA construction and transfection**

614 The pLVX-shRNA-puro lentivirus vector carrying shRNA was constructed by Shanghai
615 OBiO Technology Inc. for targeted gene knockdown in vitro. The pAAV-U6-shRNA-CMV-
616 MCS-WPRE adeno-associated virus (AAV) vector carrying shRNA was constructed by
617 Shanghai OBiO Technology Inc. for targeted gene knockdown in vivo. The shRNA sequences
618 used are *shARL3:* 5'-AAGCTGAATGTATGGGACATT-3'; *shIFT88*: 5'-
619 GCCCTCAGATAGAAAGACCAA-3'; *shMest*: 5'-CACCGGCCATTGGATCCTAT-3' ;*shNC*:
620 5'-CCTAAGGTTAAGTCGCCCTCG-3'.
621 Forty-eight hours after tHO induction in mice, 10 μL of the AAV was injected
622 intramuscularly into the medial side of the injured hind limb. Subsequent injections were
623 administered every 3–5 days to achieve sustained knockdown of the specific gene expression.
624 For lentivirus-mediated transduction in TSPCs, 8×10^4 cells were seeded into each well of a 6-
625 well plate. When the cell density reached 20%–30%, cells were transduced with lentivirus in the
626 presence of polybrene (8–10 hours). Subsequently, stable transduced cells were selected using 2
627 μg/ml puromycin for 5–10 days. The successful establishment of stable cell lines was verified by
628 quantitative qPCR and Western blot.

The siRNA targeting MEST gene (*siMest-1*: 5'-UGGUCAUCCAGAAUCGACACUGUGG-3'; *siMest-2*: 5'-GAGGAUCCCAUGGGCUUCUUGAAUG-3') and nontargeting control siRNA (*siNC*: 5'-UGGGUUCUACAGACGCUACACAUGG-3') was synthesized by Shanghai GenePharma. For siRNA transfection, 1×10^5 cells were seeded into each well of a 6-well plate. When the cell density reached 50%, cells were transfected with siRNA using Lipofectamine RNAiMAX (Invitrogen). Specifically, the siRNA was mixed with Lipofectamine RNAiMAX and incubated at room temperature for 10 minutes. The mixture was then added to cells cultured in Opti-MEM reduced-serum medium. After incubation for 48–72 hours, cells were harvested for subsequent experiments.

7. Induction of TSPCs osteogenic and chondrogenic differentiation

To induce osteogenic differentiation of TSPCs, gelatin-coated 6-well plates were used to promote cell attachment and growth. TSPCs were seeded at a density of 1×10^4 cells/cm^2 and cultured in osteogenic induction medium containing 10 mM β-glycerophosphate, 50 μg/ml ascorbic acid, and 100 nM dexamethasone. The medium was changed every 2-3 days to maintain optimal conditions. Osteogenic differentiation was assessed by alizarin red staining after 2-4 weeks to visualize calcium deposits. Additionally, qPCR was performed to evaluate the expression of osteogenesis related genes.

To induce chondrogenic differentiation of TSPCs, cells were seeded at a density of 1×10^4 cells/cm^2 on gelatin-coated 6-well plates and cultured in chondrogenic induction medium containing 10 ng/ml transforming growth factor-β3 (TGF-β3), 100 nM dexamethasone, 50 μg/ml ascorbic acid, and 10 mM β-glycerophosphate. The medium was refreshed every 2-3 days to ensure optimal conditions for differentiation. Chondrogenic differentiation was assessed by histological staining with alcian blue to detect glycosaminoglycans at 2-4 weeks. qPCR was also performed to evaluate the expression of chondrogenic markers.

8. Quantitative polymerase chain reaction (qPCR)

To assess the mRNA levels of the target genes, total RNA was purified from TSPCs using an RNA Easy Fast Tissue/Cell Kit (#DP451, TIANGEN). The extracted mRNA was reverse-transcribed into cDNA using FastKing gDNA Dispelling RT SuperMix (#KR118, TIANGEN). Quantitative PCR was performed using the ABI Step One Plus system (Applied Biosystems). Each reaction mixture (final volume of 20 μL) contained 1 μL of total cDNA, Power SYBR Green PCR Master Mix (#A57155, Invitrogen), and gene-specific primers. The PCR protocol included an initial denaturation at 95°C for 10 minutes, followed by 45 cycles of 95°C for 20 seconds, 72°C for 30 seconds, and a final dissociation curve analysis from 60°C to 95°C at a heating rate of 0.1°C per second. GAPDH was used as an internal control. Relative gene expression was calculated using the $2^{-\Delta\Delta Ct}$ method. Primers used in the study are listed as follows: *Shh* (F: 5'-CTGGCTCGCCTGGCTGTG-3'; R: 5'-CCACGGAGTTCTCTGCTTTCAC-3'); *Ptch1* (F: 5'-GGCTGGCTGGCGTCCTG-3'; R: 5'-CATCATCCACACCAACACCAAGAG-3'); *Alpl* (F: 5'-CACGGCGTCCATGAGCAGAAC-3'; R: 5'-CAGGCACAGTGGTCAAGGTTGG-3'); *Runx2* (F: 5'-TCCCAGGCAGGCACAGTCTTC-3'; R: 5'-AGCGGCGTGGTGGAGTGG-3'); *Bglap* (F: 5'-AGGGCAGCGAGGTAGTGAAGAG-3'; R: 5'-GCCGATGTGGTCAGCCAACTC-3'); *Sp7* (F: 5'-CCTCTGCGGGACTCAACAAC-3'; R: 5'-AGCCCATTAGTGCTTGTAAAGG-3'); *Col2a1* (F: 5'-GGTCCTCCTGGTCCTGGCATC-3'; R: 5'-CGTGCTGTCTCAAGGTACTGTCTG-3'); *Sox9* (F: 5'-

674 ATGACCGACGAGCAGGAGAAGG-3'; R: 5'-CCGAGGGACAGGGCGAACC-3'); *Acan* (F:
675 5'-GGAGACCCAGACAGCAGAAACAAC-3'; R: 5'-GCAGGTGGCTCCATTCAGACAAG-
676 3'); *Ift88* (F: 5'-TTCAGCAAGCAGTGAGAACCAGTC-3'; R: 5'-
677 TGTCCCTGTCATCGGTCTTCCC-3'); *Arl3* (F: 5'-TGTGTGCCCGTGCTCATCTTTG-3'; R:
678 5'-TGGACGCCCTCGCCTGTG-3'); *Gli2* (F: 5'-GCTCCACACACCCGCAACAC-3'; R: 5'-
679 CTCAGCATCGTCACTTCGGTCAG-3'); *Mest* (F: 5'-CTTAGGCTTTGGCTTCAGTGACAA-
680 3'; R: 5'-AGGTTGATTCTGCGGTTCTGGAG-3');
681
682 **9. Western blot**

683 To perform western blot analysis, proteins were extracted from cells by washing with PBS,
684 lysing in RIPA buffer (#R0278, Sigma-Aldrich) containing Protease & Phosphatase Inhibitor
685 Cocktail (#78441, Thermo Fisher Scientific), and sonicating on ice. The lysates were centrifuged
686 at 4°C to collect the supernatant, and protein concentrations were determined using a BCA
687 Protein Assay Kit (#P0011, Beyotime). Equal amounts of protein were denatured by heating in
688 SDS loading buffer, separated by SDS-PAGE, and transferred to PVDF or nitrocellulose
689 membranes. Membranes were blocked with 5% skim milk in TBST to reduce nonspecific
690 binding. Primary antibodies were applied overnight at 4°C, followed by washing and incubation
691 with secondary antibodies conjugated to horseradish peroxidase (#SA00001-2, Proteintech Inc.)
692 for 1 hour at room temperature. After additional washing, the membranes were developed using
693 Super ECL Detection Reagent (#36208ES60, YEASEN) and imaged with ChemiDoc XRS+ Gel
694 Imaging System (Bio-Rad). Band intensities were quantified using ImageJ software, and target
695 protein expression levels were normalized to those of the internal control. Primary antibodies
696 used in western blot are as follows: MEST (1:1000, #11118-1-AP, Proteintech Group Inc.), GLI2
697 (1:2000, #28245-1-AP, Proteintech Group Inc.), PTCH1 (1:1000, #ab53715, abcam), SHH
698 (1:2000, #20697-1-AP, Proteintech Group Inc.), IFT88 (1:6000, #13967-1-AP, Proteintech
699 Group Inc.), ARL3 (1:1000, #10961-1-AP, Proteintech Group Inc.), PI3K (1:1000, #ab191606,
700 abcam), p-PI3K (1:2000, #ab278545, abcam), AKT (1:2000, #ab8805, abcam), p-AKT (1:1000,
701 #ab38449, abcam).
702
703 **10. RNA-seq**

704 Total RNA was isolated from samples using RNA Easy Fast Tissue/Cell Kit (#DP451,
705 TIANGEN). The purity and concentration of the extracted RNA were assessed using the
706 NanoDrop One spectrophotometer (Thermo Fisher Scientific). RNA integrity was further
707 evaluated using the Agilent 2100 Bioanalyzer (Agilent Technologies). Subsequently, RNA
708 sequencing libraries were prepared using the VAHTS Universal V6 RNA-seq Library Prep Kit
709 (Vazyme). The transcriptome sequencing and subsequent bioinformatics analysis were
710 performed by Shanghai OE Biotech. Sequencing libraries were sequenced on the Illumina
711 Novaseq 6000 platform to generate 150-bp paired-end reads. The raw sequencing reads in
712 FASTQ format were processed using the fastp software to remove low-quality reads, yielding
713 clean reads for subsequent data analysis. The clean reads were aligned to the reference genome
714 using the HISAT2 software, and gene expression levels were calculated in terms of fragments
715 per kilobase of transcript per million mapped reads (FPKM). Additionally, read counts for each
716 gene were obtained using HTSeq-count. Subsequent analyses, including principal component
717 analysis (PCA), differential gene expression analysis, and enrichment analysis, were performed
718 using the R software.

11. Untargeted lipidomics using liquid chromatography-tandem mass spectrometry (LC-MS/MS)

TSPCs were cultured in serum-free medium to promote cilium growth until confluence. The cells were washed with PBS and subjected to shear force by rotating at 360 rpm in a shaking incubator at 37°C for 4 minutes to detach cilia as previously reported(*37*). The cell debris was removed by centrifugation at 1000×g for 10 minutes at 4°C, followed by ultracentrifugation at 40,000×g for 30 minutes at 4°C to isolate the ciliary suspension from the supernatant. The ciliary suspension was then used for untargeted lipidomics sequencing.

For lipid extraction, 200 μL of pre-chilled methanol/water (3:1, v/v) was added to the ciliary suspension, followed by sonication on ice for 15 minutes. Then, 1 mL of pre-chilled methyl tert-butyl ether (MTBE) was added and vortexed thoroughly. The mixture was rotated at 4°C for 1 hour, followed by sonication on ice for another 30 minutes. After adding 100 μL of water and vortexing for 1 minute, the mixture was left at room temperature for 10 minutes. The sample was then centrifuged at 14,000×g for 15 minutes at 4°C. The supernatant was collected, and the pellet was dried under a stream of nitrogen. The dried pellet was re-dissolved in 200 μL of SDT buffer. Protein concentration was measured using the BCA assay (Table 4-2). Based on the protein content, the cell quantity in each sample was estimated, and equal cell amounts were taken from each supernatant. The supernatant was dried using a high-speed vacuum concentrator, re-dissolved in 60 μL of pre-chilled isopropanol/methanol (1:1, v/v), and centrifuged at 20,000×g for 20 minutes at 4°C. The supernatant was vortexed and transferred to an injection vial for analysis. The entire analysis was performed at 4°C using an automatic sampler. The samples were analyzed using a SHIMADZU-LC30 ultra-high-performance liquid chromatography (UHPLC) system equipped with an ACQUITY UPLC® HSS C18 column (2.1×100 mm, 1.9 μm) (Waters, Milford, MA, USA). To avoid signal drift, samples were analyzed in a random order. A quality control (QC) sample was inserted every 5-10 experimental samples to monitor system stability and data reliability. The samples were analyzed in both positive and negative ion modes using electrospray ionization (ESI). After separation by UHPLC, the samples were analyzed using a QExactive Plus mass spectrometer (Thermo Fisher Scientific). Lipid identification and quantification were performed using the MSDIAL software (Version 5.2.240218.2-net472) with the following parameters: precursor mass tolerance of 10 ppm, product mass tolerance of 10 ppm, retention time alignment of 0.1 min, and peak area filtering to reduce false positives. Lipids with relative standard deviations (RSD) exceeding 30% in QC samples were excluded. The data were normalized to the total peak area, preprocessed with UV-scaling, and subjected to multivariate statistical analyses, including unsupervised principal component analysis (PCA), supervised partial least squares discriminant analysis (PLS-DA), and orthogonal partial least squares discriminant analysis (OPLS-DA). Univariate statistical analyses included Student's t-test and fold-change analysis, and volcano plots and hierarchical clustering were generated using R software.

12. Dual-luciferase reporter assay

The Dual-Luciferase Reporter Assay was performed using the Dual-Luciferase Reporter Assay System (Promega). The firefly luciferase reporter gene was cloned downstream of the wild-type (WT) or mutant (MUT) pGL4.10-Mest promoter regions and co-transfected into TSPCs with pcDNA3.1-GLI2 and Renilla expression vector pRL-TK. Following a 48-hour

incubation, cell lysates were prepared, and firefly luciferase activity was quantified and normalized to Renilla luciferase activity as an internal control.

13. Bioinformatics analysis

The scRNA sequencing dataset pertaining to tHO in mice was retrieved from the GEO database (GSE126060). Dimensionality reduction, clustering, and cell-type identification of the scRNA sequencing data were performed using the Seurat package in R software. Additionally, bulk RNA sequencing data from the heterotopic ossification sites of mice three weeks post-trauma was also obtained from the GEO database (GSE233201). Differential gene expression analysis was conducted using the DESeq2 package, while enrichment analysis was performed with the clusterProfiler package. Transcription factor binding sites were predicted using the JASPAR database (https://jaspar.elixir.no/).

14. Statistical analysis

All statistical analyses were performed using SPSS software and R Studio. Data are presented as mean ± standard deviation (SD) of three independent assays. Statistical analyses were performed by Student's t-test for two-group comparison and one-way ANOVA analyses with Tukey's post hoc test for multiple comparisons. Statistical significance was set at $P < 0.05$.

List of Supplementary Materials

Fig. S1 to S8 for multiple supplementary figures

Table S1 to S2 for multiple supplementary tables (Excel files)

References and Notes

1. D. Dey *et al.*, The traumatic bone: trauma-induced heterotopic ossification. *Transl Res* **186**, (2017).
2. K. Ranganathan *et al.*, Heterotopic Ossification: Basic-Science Principles and Clinical Correlates. *The Journal of Bone and Joint Surgery. American Volume* **97**, 1101-1111 (2015).
3. P. Mill, S. T. Christensen, L. B. Pedersen, Primary cilia as dynamic and diverse signalling hubs in development and disease. *Nature Reviews. Genetics* **24**, 421-441 (2023).
4. Z. Anvarian, K. Mykytyn, S. Mukhopadhyay, L. B. Pedersen, S. T. Christensen, Cellular signalling by primary cilia in development, organ function and disease. *Nature Reviews. Nephrology* **15**, 199-219 (2019).
5. M. Spasic, M. P. Duffy, C. R. Jacobs, Fenoldopam Sensitizes Primary Cilia-Mediated Mechanosensing to Promote Osteogenic Intercellular Signaling and Whole Bone Adaptation. *J Bone Miner Res* **37**, 972-982 (2022).
6. K. He *et al.*, Primary cilia mediate skeletogenic BMP and Hedgehog signaling in heterotopic ossification. *Sci Transl Med* **16**, eabn3486 (2024).
7. C. D. Hwang *et al.*, Contemporary perspectives on heterotopic ossification. *JCI Insight* **7**, (2022).
8. Y. Bi *et al.*, Identification of tendon stem/progenitor cells and the role of the extracellular matrix in their niche. *Nat Med* **13**, 1219-1227 (2007).
9. G. Dai *et al.*, Higher BMP Expression in Tendon Stem/Progenitor Cells Contributes to the Increased Heterotopic Ossification in Achilles Tendon With Aging. *Front Cell Dev Biol* **8**, 570605 (2020).
10. Y. Chen *et al.*, Targeted pathological collagen delivery of sustained-release rapamycin to prevent heterotopic ossification. *Sci Adv* **6**, eaay9526 (2020).
11. P. Dutta, K. Ray, Ciliary membrane, localised lipid modification and cilia function. *Journal of Cellular Physiology* **237**, 2613-2631 (2022).
12. C. Iwaya, A. Suzuki, J. Iwata, Loss of Sc5d results in micrognathia due to a failure in osteoblast differentiation. *J Adv Res* **65**, 153-165 (2024).
13. A. Suzuki *et al.*, Disruption of Dhcr7 and Insig1/2 in cholesterol metabolism causes defects in bone formation and homeostasis through primary cilium formation. *Bone Research* **8**, 1 (2020).

14. L. Nikonova *et al.*, Mesoderm-specific transcript is associated with fat mass expansion in response to a positive energy balance. *FASEB Journal : Official Publication of the Federation of American Societies For Experimental Biology* **22**, 3925-3937 (2008).
15. A. K. Huber *et al.*, Immobilization after injury alters extracellular matrix and stem cell fate. *The Journal of Clinical Investigation* **130**, 5444-5460 (2020).
16. K. Noda, M. Kitami, K. Kitami, M. Kaku, Y. Komatsu, Canonical and noncanonical intraflagellar transport regulates craniofacial skeletal development. *Proc Natl Acad Sci U S A* **113**, E2589-2597 (2016).
17. H. Feng *et al.*, Tendon-derived cathepsin K-expressing progenitor cells activate Hedgehog signaling to drive heterotopic ossification. *The Journal of Clinical Investigation* **130**, 6354-6365 (2020).
18. S. Chen *et al.*, A CD26+ tendon stem progenitor cell population contributes to tendon repair and heterotopic ossification. *Nat Commun* **16**, 749 (2025).
19. J. B. Regard *et al.*, Activation of Hedgehog signaling by loss of GNAS causes heterotopic ossification. *Nat Med* **19**, 1505-1512 (2013).
20. K. Ha *et al.*, Cilia-enriched oxysterol 7β,27-DHC is required for polycystin ion channel activation. *Nat Commun* **15**, 6468 (2024).
21. D. Yamakawa *et al.*, Primary cilia-dependent lipid raft/caveolin dynamics regulate adipogenesis. *Cell Reports* **34**, 108817 (2021).
22. M. Pekkinen *et al.*, Osteoporosis and skeletal dysplasia caused by pathogenic variants in SGMS2. *JCI Insight* **4**, (2019).
23. G. Luchetti *et al.*, Cholesterol activates the G-protein coupled receptor Smoothened to promote Hedgehog signaling. *ELife* **5**, (2016).
24. M. Kinnebrew *et al.*, Cholesterol accessibility at the ciliary membrane controls hedgehog signaling. *ELife* **8**, (2019).
25. S. P. Taylor *et al.*, Mutations in DYNC2LI1 disrupt cilia function and cause short rib polydactyly syndrome. *Nat Commun* **6**, 7092 (2015).
26. H. Chen *et al.*, The effects of primary cilia-mediated mechanical stimulation on nestin+-BMSCs during bone-tendon healing. *J Adv Res*, (2024).
27. D. Tao *et al.*, Primary cilia support cartilage regeneration after injury. *Int J Oral Sci* **15**, 22 (2023).
28. X. Liu *et al.*, Numb positively regulates Hedgehog signaling at the ciliary pocket. *Nat Commun* **15**, 3365 (2024).
29. B. A. Allard *et al.*, Thm2 interacts with paralog, Thm1, and sensitizes to Hedgehog signaling in postnatal skeletogenesis. *Cell Mol Life Sci* **78**, 3743-3762 (2021).
30. Q. Cong *et al.*, A self-amplifying loop of YAP and SHH drives formation and expansion of heterotopic ossification. *Sci Transl Med* **13**, (2021).
31. X. Yuan, M. Liu, X. Cao, S. Yang, Ciliary IFT80 regulates dental pulp stem cells differentiation by FGF/FGFR1 and Hh/BMP2 signaling. *International Journal of Biological Sciences* **15**, 2087-2099 (2019).
32. V. Jou, S. M. Peña, J. A. Lehoczky, Regeneration-specific promoter switching facilitates Mest expression in the mouse digit tip to modulate neutrophil response. *NPJ Regen Med* **9**, 32 (2024).
33. W. Lu *et al.*, Hedgehog signaling regulates bone homeostasis through orchestrating osteoclast differentiation and osteoclast-osteoblast coupling. *Cell Mol Life Sci* **80**, 171 (2023).
34. Y. Wang *et al.*, TMEM216 promotes primary ciliogenesis and Hedgehog signaling through the SUFU-GLI2/GLI3 axis. *Sci Signal* **17**, eabo0465 (2024).
35. J. R. Peterson *et al.*, Direct Mouse Trauma/Burn Model of Heterotopic Ossification. *J Vis Exp*, e52880 (2015).
36. M. Chen *et al.*, Noncanonical Wnt5a signaling regulates tendon stem/progenitor cells senescence. *Stem Cell Res Ther* **12**, 544 (2021).
37. D. R. Raleigh *et al.*, Cilia-Associated Oxysterols Activate Smoothened. *Mol Cell* **72**, (2018).

Acknowledgments: We thank Airu Zhu at Shanghai Bioprofile Technology CompanyLtd for her technical support in mass spectroscopy.

Funding: National Natural Science Foundation of China 82302084 (HJ)

Author contributions:

Conceptualization: HJ, XHZ

Methodology: BWL, JQZ
Investigation: BWL, YG
Visualization: BWL, ZLS
Funding acquisition: HJ
Project administration: HJ, XHZ
Supervision: JQZ
Writing – original draft: BWL, YG
Writing – review & editing: HJ, XHZ

Competing interests: Authors declare that they have no competing interests.

Data and materials availability: The data that support the findings of this study are available from corresponding author upon reasonable request. Publicly available datasets were analyzed in this study, these can be found in Gene Expression Omnibus (GSE126060 and GSE233201) of National Center for Biotechnology Information.

Ethical approval : All animal procedures were conducted in accordance with the guidelines of the Ethics Committee on Animal Experiments of the Naval Medical University.

Figures

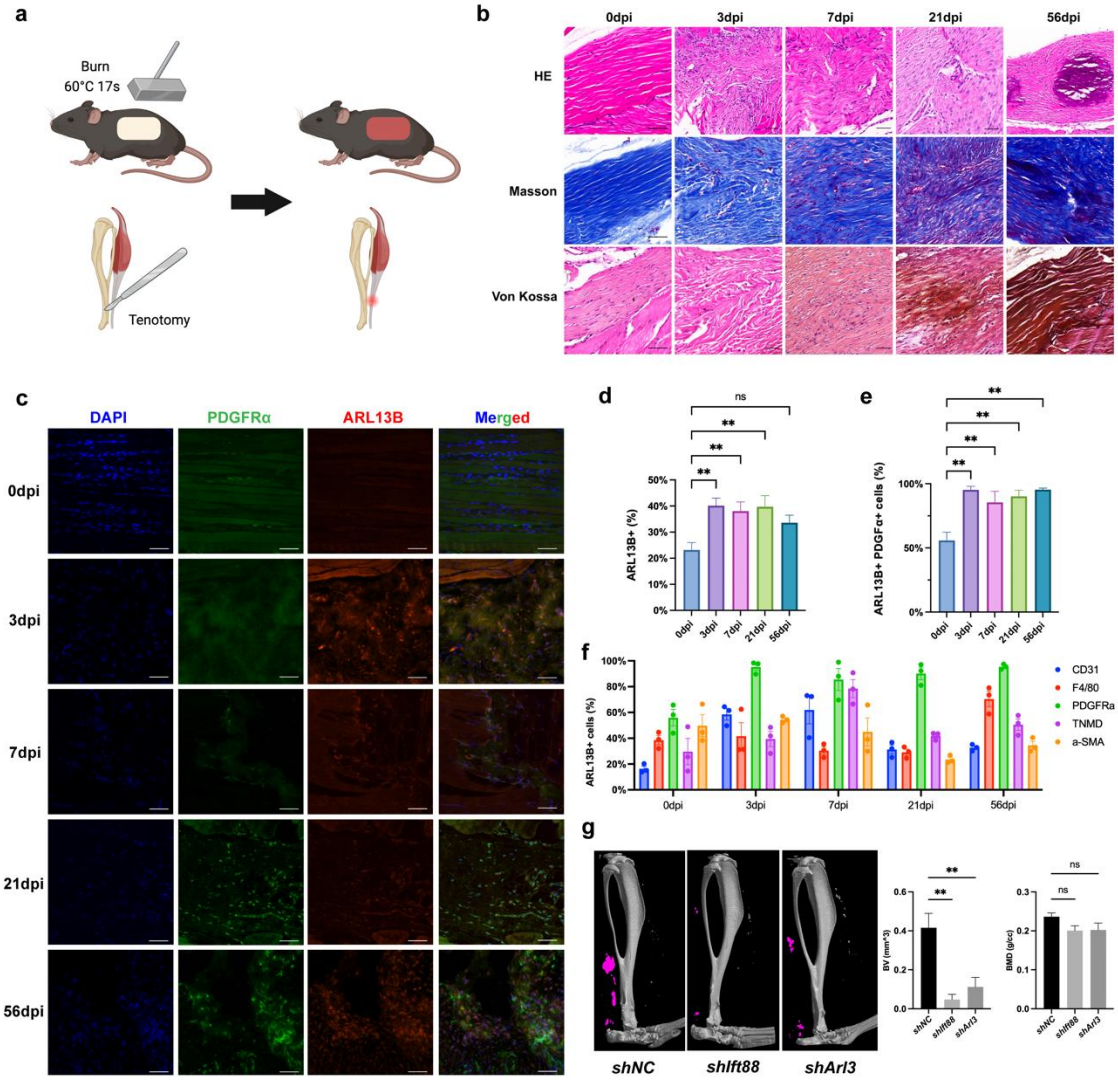

Figure 1. Primary cilia defects rescue the ecotopic bone formation of tHO. (a) Illustration of establishment of the tHO burn/tenotomy mouse model. (b) HE, Masson trichrome, and Von Kossa staining of tHO tendon tissues collected from differnet time points after injury (scale bar 50 um). (c) Immunofluorescence images of PDGFRα (green) and ARL13B (red) at differnet time points during tHO development. DAPI staining indicates nuclei (blue), scale bar 50 um. (d) The percentage of ARL13B+ cells at differnet time points after injury are shown. Data are presented as means ± SD (n= 3). (e) The percentage of ARL13+ cells in PDGFRα+ cells are shown (n= 3). (f) The percentage of ARL13+ cells in five types of cells (CD31+, F4/80+, PDGFRα+, TNMD+, and α-SMA+ cells) are shown (n= 3). (g) Micro-CT images show tHO of lower limbs among *shNC, shIFT88*, and *shARL3* groups (n= 4/group). Bone volume (BV, mm^3), bone mineral dendity (BMD, g/cc), and Tb.Th (trabecular thickness, mm) are quantificated. Data are presented as means ± SD of three independent assays. Statistical analyses were performed by one-way ANOVA analyses with Tukey's post hoc test for multiple comparisons. **P < 0.01; ns, P > 0.05.

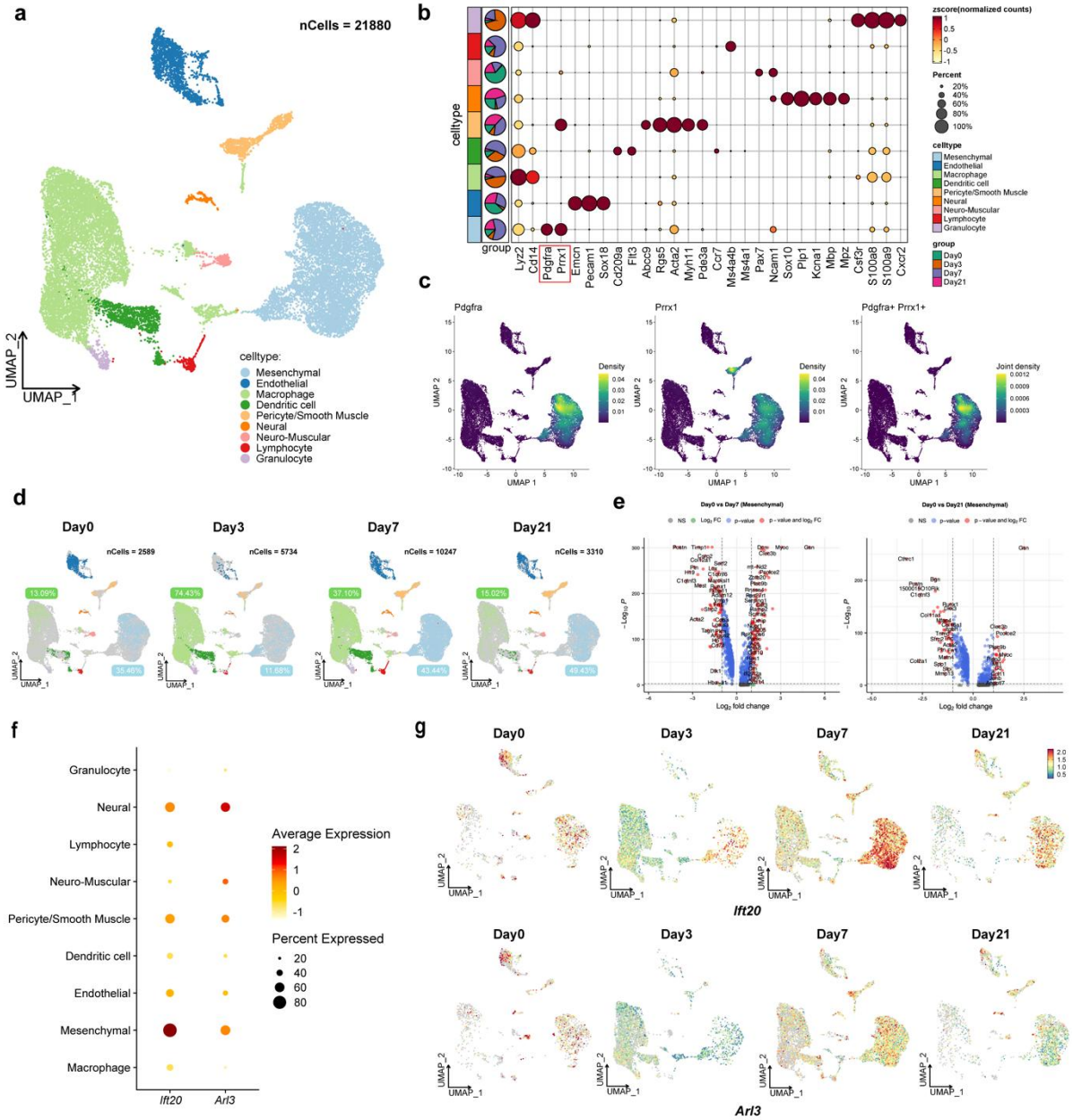

Figure 2. scRNA-seq indicated the potential role of cilia and stem/progenitor cells in tHO development. (a) UMAP plot of nine clusters identified in 21880 cells in total of tHO site. (b) Bubble plot shows the high variable marker genes of each cluster. (c) The expression density of Pdgfra+, Prrx1+, and Pdgfra+Prrx1+ cells in each cluster are shown by UMAP plot. (d) UMAP plot of nine clusters with single cells grouped by different tim points (Day0 ,3, 7, 21) during tHO demonstrates the trend of changes in cell composition. (e) The volcano plot visualizes the differential expressed genes in the Mesenchymal subcluster at Day 7 (left) or Day 21 (right) compared to the Day 0 group. (f) The dot plot visualizes the different expression of *Ift20* and *Arl3* in nine clusters. (g) UMAP plot shows the expression of *Ift20* (upper) and *Arl3* (lower) at different time points (Day0 ,3, 7, 21) during tHO development.

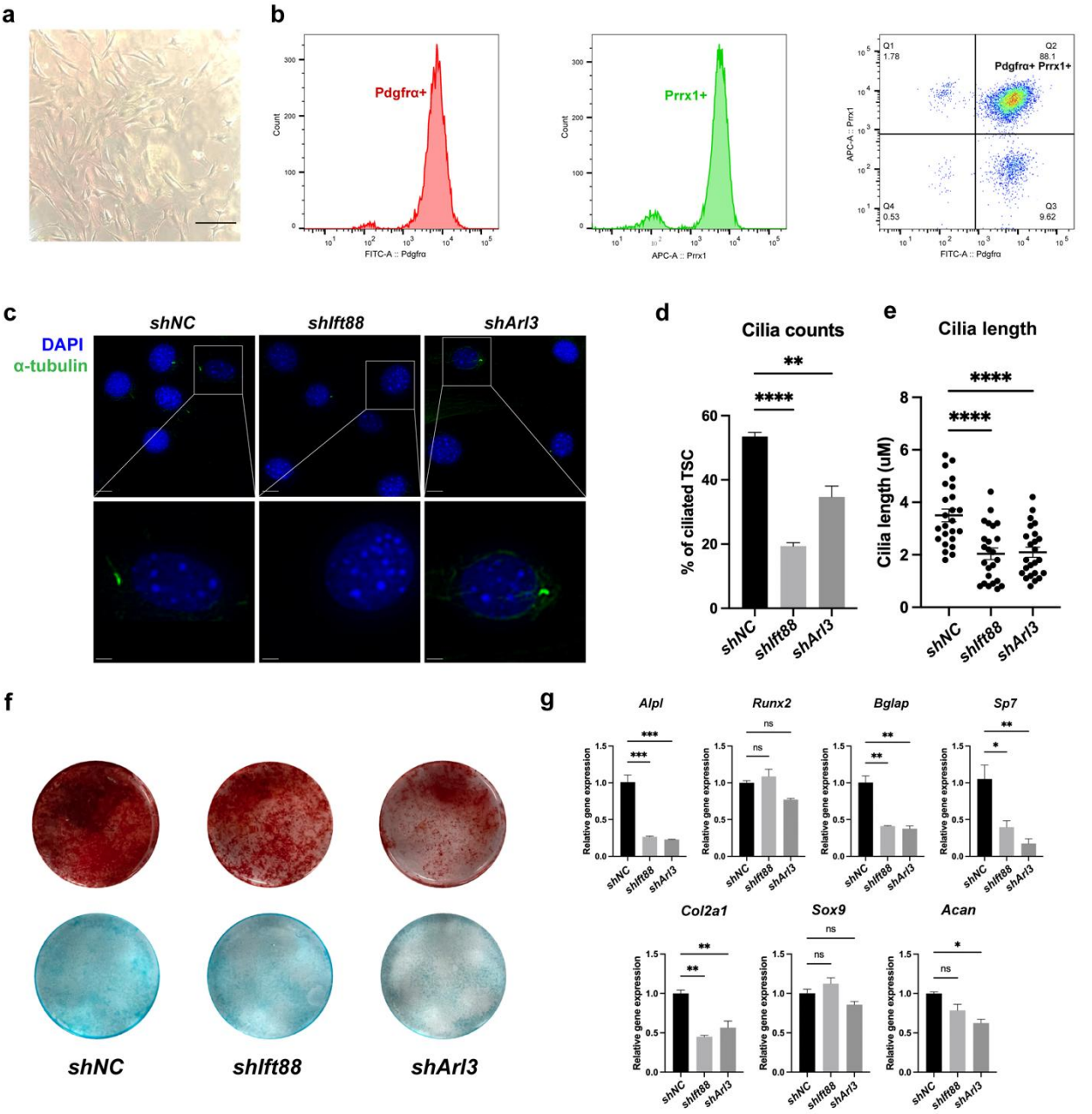

Figure 3. TSPCs osteochondrogenic differentiation is regulated by primary cilia in tHO. (a) Fibroblast-like TSPCs extracted from mice for subsequent experiments (scale bar 100 um). (b) Flow cytometry analysis of the expression of Pdgfra and Prrx1 (stem/progenitor cell surface markers) on TSPCs. (c) Immunofluorescence images of ARL13B (red) and α-tubulin (green) mark the cilia in *shNC, shIFT88,* and *shARL3* TSPCs. DAPI staining indicates nuclei (blue), scale bar 10 um (upper) and 30 um (lower). (d) The percentage of ciliated TSPCs marked by ARL13B show the cilia counts in the control group and ciliary gene knockdown groups. (e) Cilia length in TSPCs with or without *shIFT88* or *shARL3* treatment (n= 25/group). (f) Representative images of alizarin red staining (upper) and alcian blue staining (lower) in TSPCs with or without *shIFT88* or *shARL3* treatment after 3 weeks of in vitro osteogenic or chondrogenic differentiation. (g) qPCR showed relative osteogenesis-related genes (*Alpl, Runx2, Bglap, Sp7*) and chondrogenesis-related genes (*Col2a1, Sox9, Acan*) mRNA expression in TSPCs with or without *shIFT88* or *shARL3* treatment after 3 weeks of in vitro osteogenic or chondrogenic differentiation. Data are presented as means ± SD of three independent assays. Statistical analyses were performed by one-way ANOVA analyses with Tukey's post hoc test for multiple comparisons. *P < 0.05; **P < 0.01; ***P < 0.005; ****P < 0.001. ns, P > 0.05.

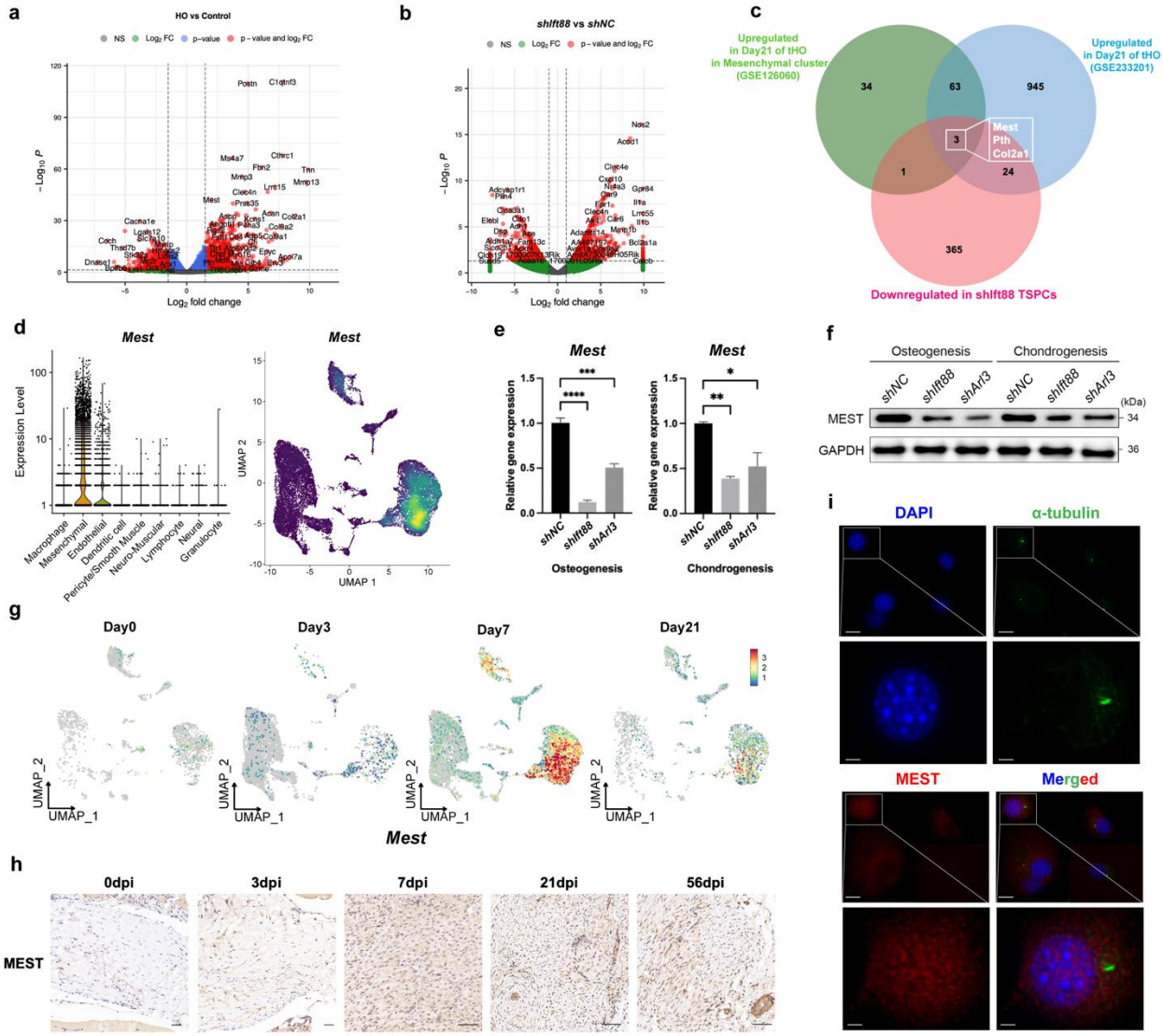

Figure 4. Primary cilia contribute to tHO pathogenesis by regulating MEST expression. (a) The volcano plot visualizes the differential expressed genes in injury site of the tHO mice 3 weeks after burn/tenotomy compared to the control mice. (b) RNA-seq performed between *shIft88* and *shNC* TSPCs after 3-7 days of in vitro osteogenic differentiation and differential expressed genes are visualized. (c) Venn diagram shows the common differential expressed genes among three genesets and identified MEST, PTN, COL2A1 as the key genes. (d) The expression density of *Mest* in each cluster are shown by violin plot and UMAP plot. (e) qPCR shows relative *Mest* mRNA expression in TSPCs with or without *shIFT88* or *shARL3* treatment during in vitro osteogenic (left) or chondrogenic (right) differentiation. (f) Western blot shows MEST protein expression levels in TSPCs with or without *shIFT88* or *shARL3* treatment during in vitro osteogenic (left) or chondrogenic (right) differentiation. (g) UMAP plot shows the expression of *Mest* at different time points (Day0 ,3, 7, 21) during tHO development. (h) Immunohistochemistry images demonstrates MEST in tHO tendon tissues at different time post burn/tenotomy injury (scale bar 100 um). (i) Immunofluorescence images of α-tubulin (green) and MEST (red) in mouse primary TSPCs. DAPI staining indicates nuclei (blue), scale bar 10 um. Data are presented as means ± SD of three independent assays. Statistical analyses were performed by one-way ANOVA analyses with Tukey's post hoc test for multiple comparisons. *P < 0.05; **P < 0.01; ***P < 0.005; ****P < 0.001.

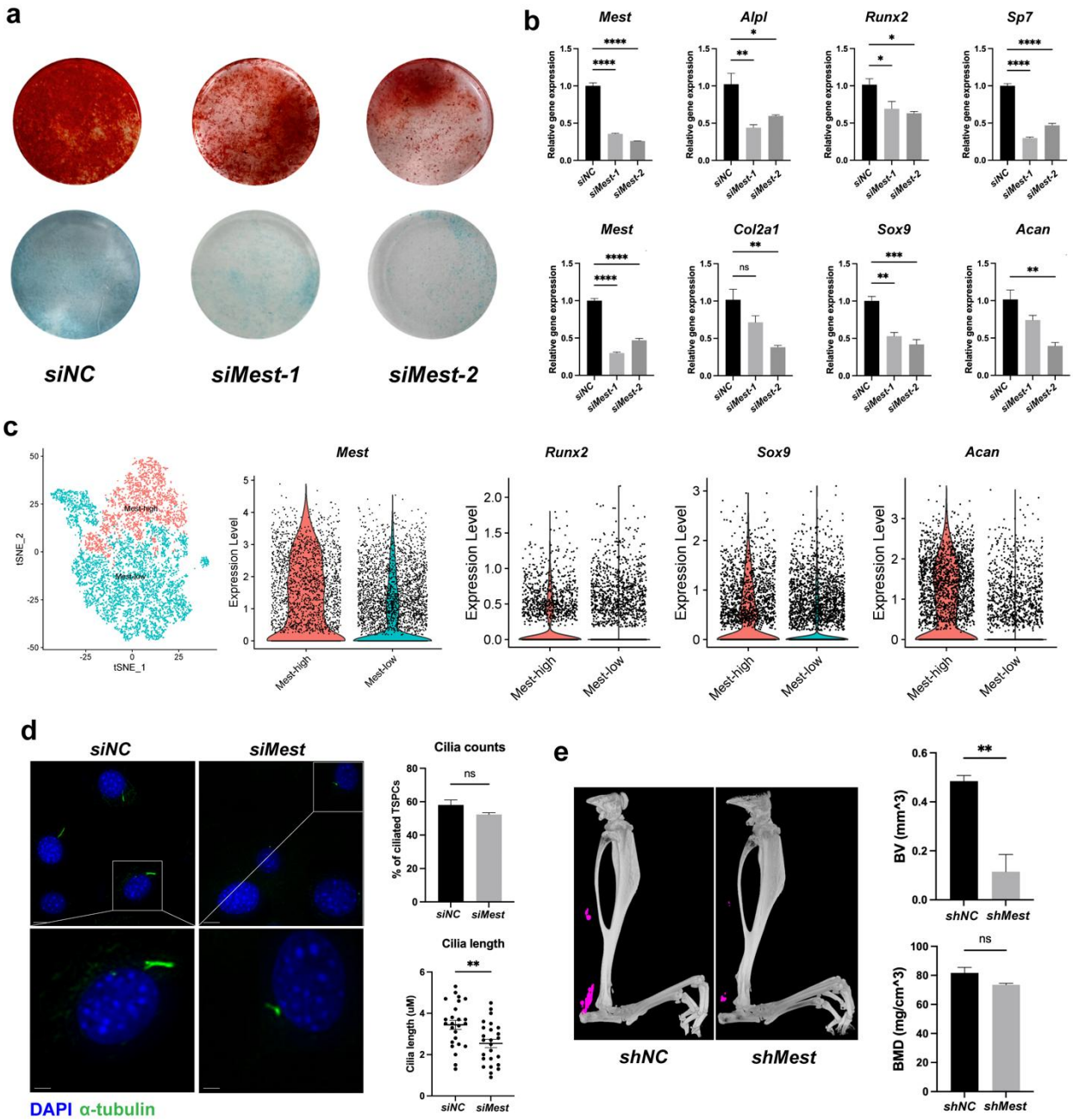

Figure 5. MEST modulates TSPCs cilia length and osteochondral differentiation in tHO. (a) Representative images of alizarin red staining (upper) and alcian blue staining (lower) in TSPCs with or without *siMest* treatment after 3 weeks of in vitro osteogenic or chondrogenic differentiation. (b) qPCR shows relative *Mest* and osteogenic differentiation-related (*Alpl, Runx2, Bglap*) or chondrogenic differentiation-related genes (*Col2a1, Sox9, Acan*) mRNA expression in TSPCs with or without *siMest* treatment after 3 weeks of in vitro osteogenic or chondrogenic differentiation. (c) tSNE map shows Mest-high and Mest-low subclusters divided from Mesenchymal cluster. The expression level of *Mest, Runx2, Sox9*, and *Acan* in Mest-high and Mest-low subclusters were visualize by violin plots. (d) Immunofluorescence images of α-tubulin (green) mark the cilia of TSPCs. DAPI staining indicates nuclei (blue), scale bar 10 um. Ciliated TSPCs proportion (cilia counts) marked by α-tubulin and cilia length (n= 25/group) in the *siNC* and *siMest* group. (e) Micro-CT images show tHO of lower limbs in *shNC* and *shMest* groups (n= 4/group). Quantification of tHO degree by bone volume (BV, mm^3) and bone mineral dendity (BMD, g/cc). Data are presented as means ± SD of three independent assays. Statistical analyses were performed by Student's t-test for

two-group comparison and one-way ANOVA analyses with Tukey's post hoc test for multiple comparisons. *P < 0.05; **P < 0.01; ***P < 0.005; ****P < 0.001. ns, P > 0.05.

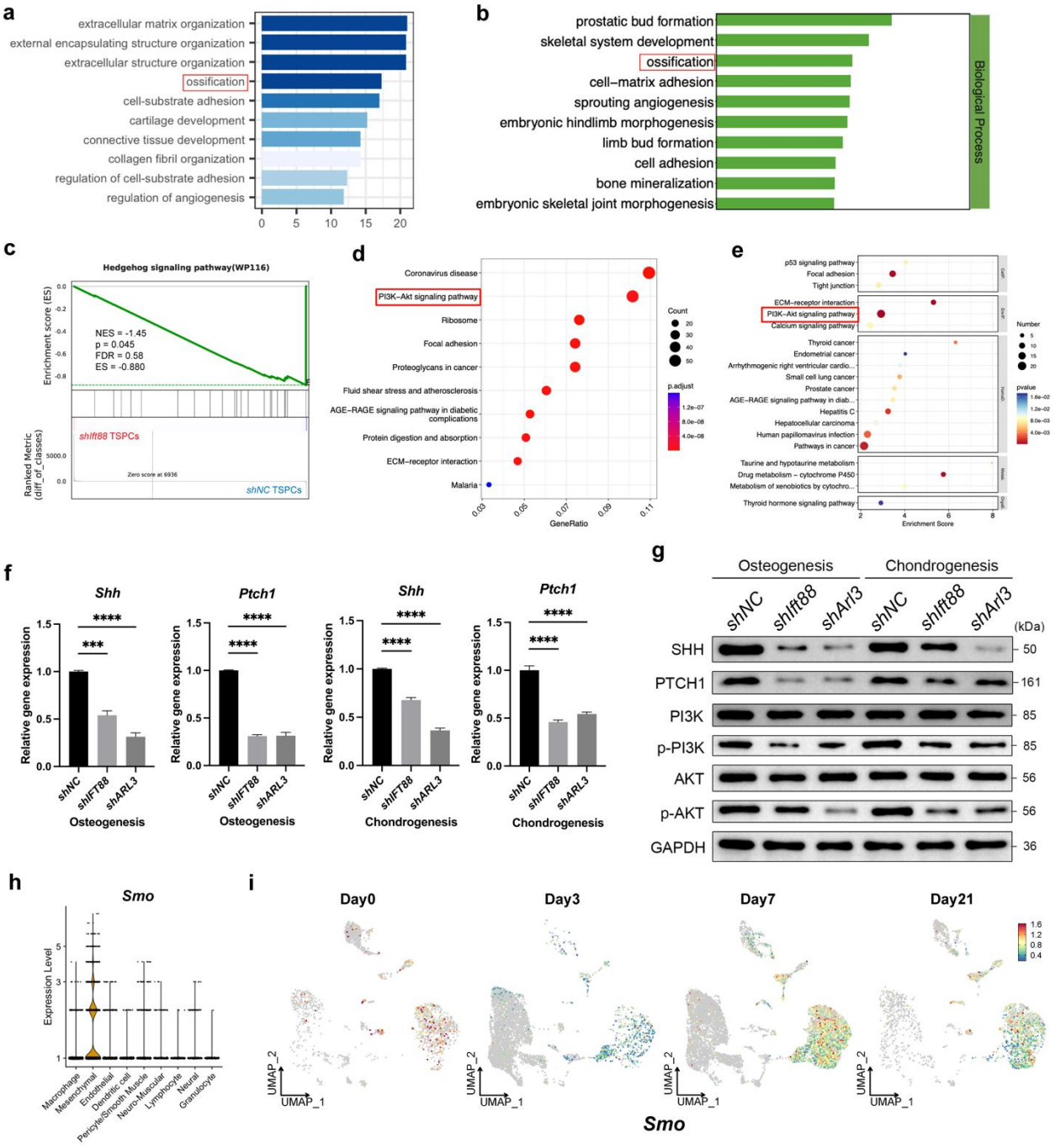

Figure 6. TSPCs ciliary Hh and PI3K-Akt signaling are involved in tHO progeression. (a) GO enrichment anaylsis of differential expressed genes in tHO mice injury site shows top 10 enriched functions that are important for tHO. (b) GO enrichment analysis of differential expressed genes in TSPCs treated with *shIft88* shows top 10 enriched biological processes. (c) GSEA enrichment of TSPCs treated with *shIft88* or *shNC*. The enriched pathway with the absolute value of normalized enrichment score (NES) greater than 1 and P-value less than 0.05 was considered significant. (d) KEGG enrichment analysis of differential expressed genes in Mesenchymal subcluster of tHO injury site identified by scRNA-seq shows top 10 enriched pathways. (e) KEGG enrichment analysis of differential expressed genes in TSPCs treated with *shIft88* showed top enriched pathways. (f) qPCR showed relative Hh signaling genes (Shh, Ptch1) mRNA expression in TSPCs with or without *shIft88* or *shARL3* treatment after 3

957 weeks of in vitro osteogenic or chondrogenic differentiation. (g) Western blot showed Hh signaling (SHH, PTCH1)
958 and PI3K-Akt signaling (PI3K, p-PI3K, AKT, p-AKT) protein expression levels in TSPCs with or without *shIFT88*
959 or *shARL3* treatment during in vitro osteogenic or chondrogenic differentiation. (h) The expression level of *Smo* in
960 each cluster are shown by violin plot. (i) UMAP plot shows the expression of *Smo* at different time points (Day0 ,3,
961 7, 21) during tHO development. Data are presented as means ± SD of three independent assays. Statistical analyses
962 were performed by one-way ANOVA analyses with Tukey's post hoc test for multiple comparisons. ***$P < 0.005$;
963 ****$P < 0.001$.

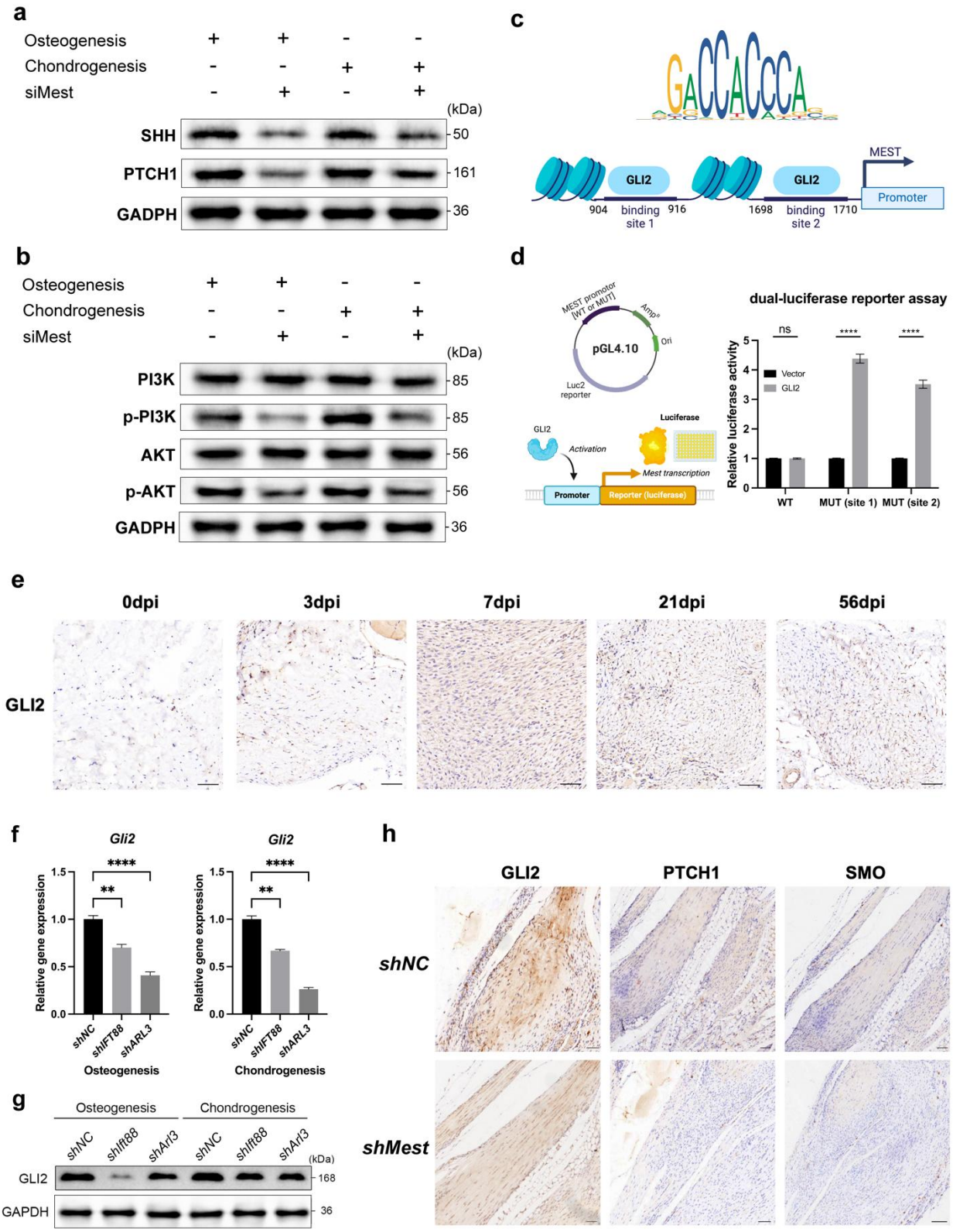

Figure 7. A self-amplifying loop of GLI2 and MEST drives TSPCs differentiation and tHO progression via Hh signaling. (a) Western blot shows Hh signaling (SHH, PTCH1) protein expression levels in TSPCs with or without *siMest* treatment during in vitro osteogenic or chondrogenic differentiation. (b) Western blot showed PI3K-Akt signaling (PI3K, p-PI3K, AKT, p-AKT) protein expression levels in TSPCs with or without *siMest* treatment

durig in vitro osteogenic or chondrogenic differentiation. (c) The sequence logo of GLI2 transcription factor and two potential binding sites of the GLI2 transcription factor on the MEST promoter region predicted by the JASPAR database. (d) The luciferase reporter assay using pGL4.10 as vector showed that GLI2 can bind to the MEST promoter at both site 1 and 2. (e) Immunohistochemistry images demonstrats GLI2 in tHO tendon tissues at different time post burn/tenotomy injury (scale bar 100 um). (f) qPCR shows relative *Gli2* mRNA expression in TSPCs with or without *shIft88* or *shARL3* treatment after 3 weeks of in vitro osteogenic or chondrogenic differentiation. (g) Western blot shows GLI2 protein expression levels in TSPCs with or without *shIFT88* or *shARL3* treatment during in vitro osteogenic or chondrogenic differentiation. (h) Immunohistochemistry images demonstrats GLI2, PTCH1, and SMO expression in tHO tendon tissues with or without shMest treatment after injury (scale bar 150 um). Data are presented as means ± SD of three independent assays. Statistical analyses were performed by one-way ANOVA analyses with Tukey's post hoc test for multiple comparisons. **P < 0.01; ****P < 0.001.

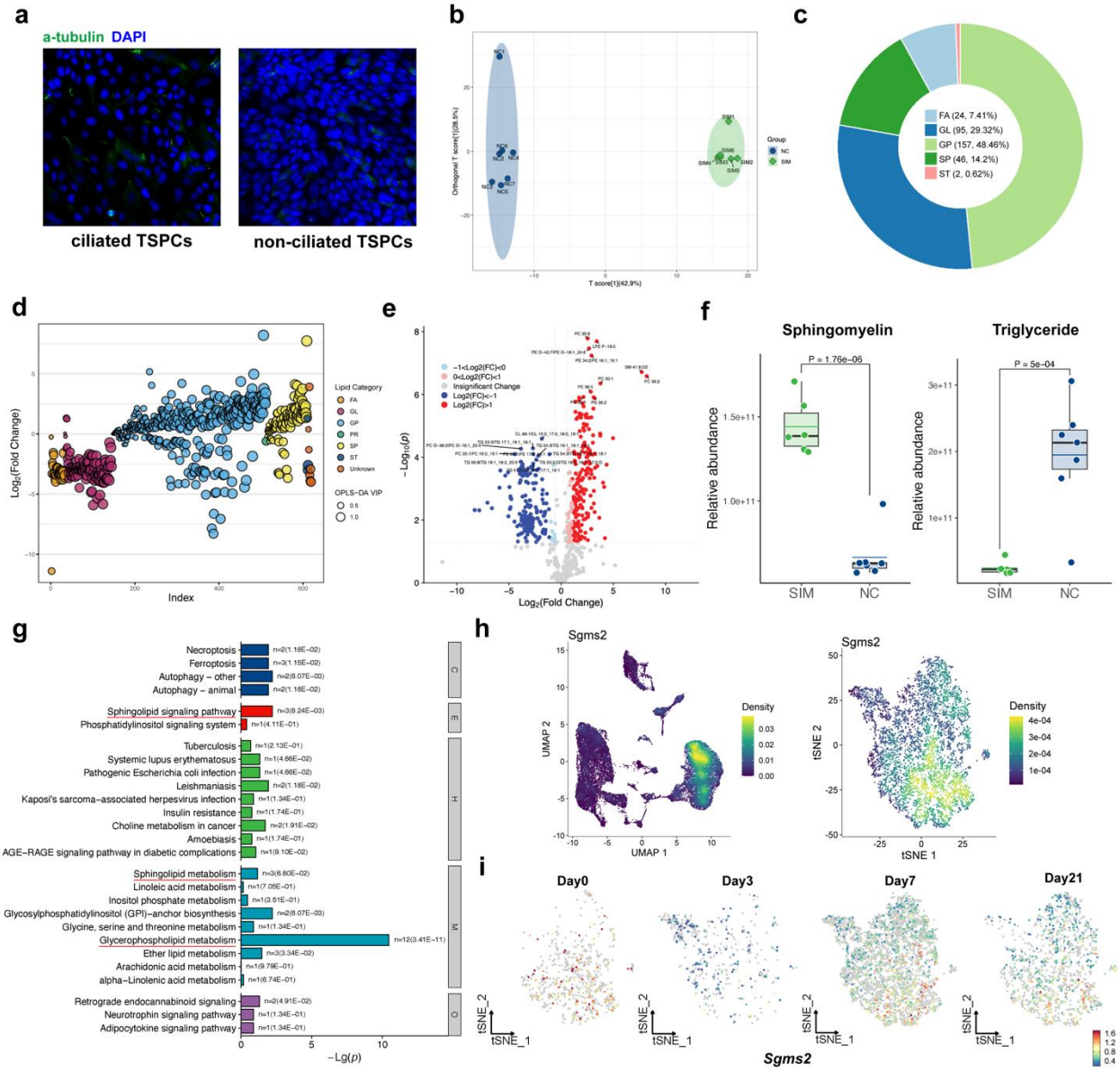

Figure 8. MEST regulates ciliary lipid metabolism in TSPCs. (a) Immunofluorescence images of α-tubulin (green) marked cilia in ciliated and non-ciliated mouse primary TSPCs after cilia isolation. DAPI staining indicates nuclei (blue). (b) OPLS-DA plot shows the differences between NC (blue, n= 7) and SIM (green, n= 6) groups. (c) Circular diagram of the classification statistics of differential lipids. (d) Bubble chart of lipid classification. The horizontal axis represents the quantity range of lipids, and the vertical axis represents the logarithmic transformation of fold change. Each circle represents a lipid substance. The larger the circle, the higher the variable importance.

Different colors represent the primary classification, and lipids of the same classification are arranged together. (e) The volcano plot visualizes the differential expressed lipids in SIM group compared to the NC group. (f) Relative abundance of sphingomyelin and triglyceride are significantly different in SIM and NC group. (g) KEGG enrichment analysis of differential expressed lipids between SIM and NC group (C: cellular processes; E: environmental information processing; H: human diseases; M: metabolism; O:organismal systems). (h) The expression density of *Sgms2* in each cluster (left) and in Mesenchymal subcluster (right) are shown by UMAP plot. (i) UMAP plot shows the expression of *Sgms2* in Mesenchymal subcluster at different time points (Day0 ,3, 7, 21) during tHO development.

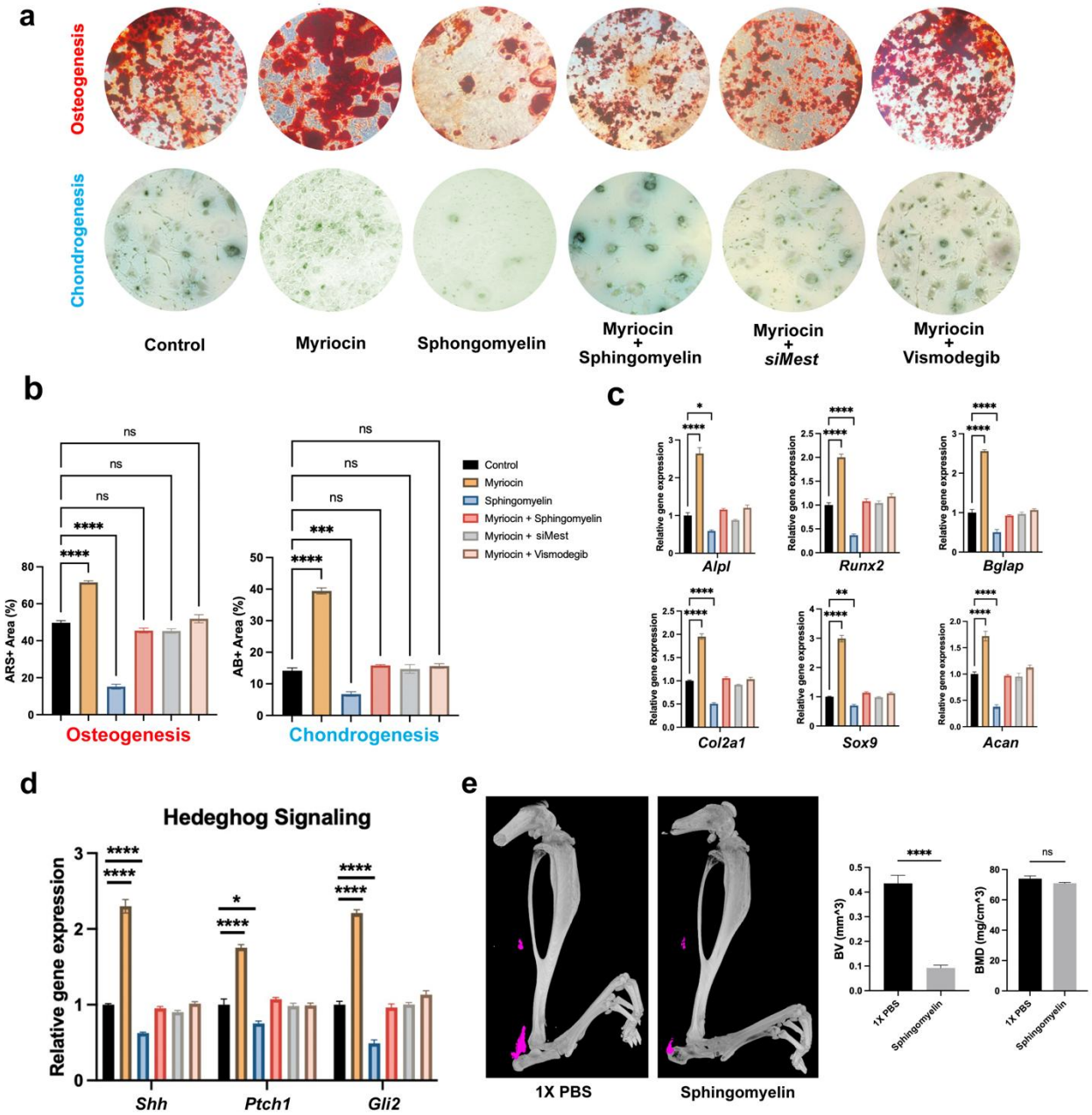

Figure 9. Targeting MEST or ciliary sphingomyelin in TSPCs may alleviate tHO via Hh signaling. (a) Representative images of alizarin red staining (upper) and alcian blue staining (lower) in TSPCs after 3 weeks of in vitro osteogenic (upper) and chondrogenic (lower) differentiation in control, myriocin, sphingomyelin, myriocin+sphingomyelin, myriocin+siMest, and myriocin+vismodegib treated groups. (b) Quantification of the percentages of (alizarin red) ARS+ and alcian blue (AB+) areas in six groups. (c) qPCR showed relative osteogenic differentiation-related genes *(Alpl, Runx2, Bglap*) and chondrogenic differentiation-related genes (*Sox9, Col2a1,*

Acan) mRNA expression in TSPCs after 3 weeks of in vitro osteogenic (upper) or chondrogenic (lower) differentiation in six groups. (d) qPCR showed relative Hh signaling genes (*Shh, Ptch1, Gli2*) mRNA expression in TSPCs after 3 weeks of in vitro osteogenic differentiation in six groups. (e) Micro-CT images show tHO of lower limbs between 1X PBS and sphingomyelin treated groups (n= 4/group). Quantification of tHO degree by bone volume (BV, mm^3) and bone mineral dendity (BMD, g/cc). Data are presented as means ± SD of three independent assays. Statistical analyses were performed by one-way ANOVA analyses with Tukey's post hoc test for multiple comparisons. *P < 0.05; **P < 0.01; ***P < 0.005; ****P < 0.001. ns, P > 0.05.

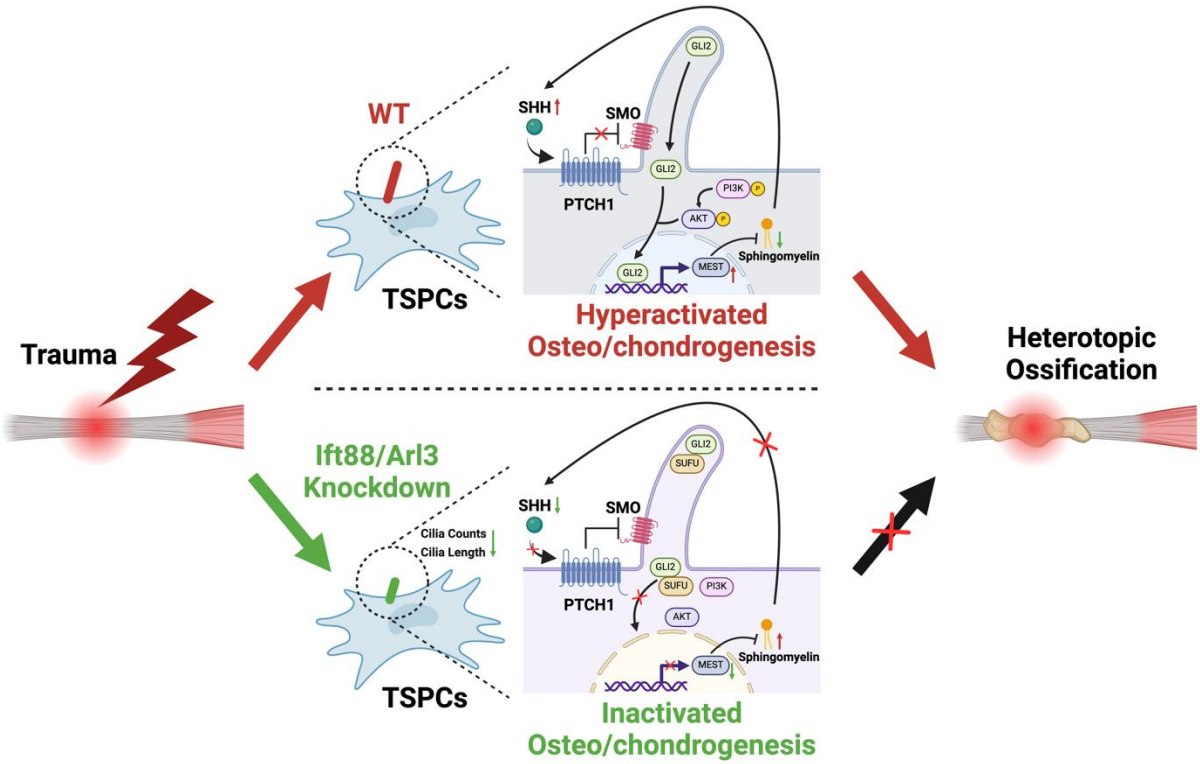

Figure 10. Schematic diagram of the study. After trauma, the level of SHH within the primary cilia of TSPCs is significantly elevated. This increase in SHH activates the Hh signaling through its interaction with PTCH1 and SMO receptors. Subsequently, the GLI2 transcription factor is activated and translocates to the nucleus, where it promotes the expression of the MEST gene. Concurrently, the phosphorylation levels of PI3K and AKT are enhanced. The upregulation of MEST expression leads to a reduction in sphingomyelin within the cilia, further amplifying the activation of the ciliary Hh signaling. This positive feedback loop dramatically enhances the osteogenic and chondrogenic differentiation potential of TSPCs, resulting in localized ectopic bone deposition and tHO. Conversely, when the ciliary genes Ift88 and Arl3 are knocked down in TSPCs, the production of SHH ligands is markedly reduced. Thus, SMO is inhibited by PTCH1, preventing the activation of GLI2. Additionally, the phosphorylation of PI3K and AKT is suppressed. The reduction in MEST expression subsequently increases the sphingomyelin within the cilia, which further inhibits the ciliary Hh signaling. As a result, the osteogenic and chondrogenic differentiation capacity of TSPCs is significantly diminished, thereby alleviating the occurrence and development of tHO.